Title

SCF^{FBXW11} complex targets interleukin-17 receptor A for ubiquitin-proteasome-mediated degradation

Author names and affiliations

Ben Jin[1,2], Sayed Ala Moududee[1,2], Dongxia Ge[3], Pengbo Zhou[4], Alun R. Wang[5], Yao-Zhong Liu[6], Zongbing You[1,2,3,7,8,9*]

[1]Southeast Louisiana Veterans Health Care System, New Orleans, Louisiana, USA; [2]Department of Structural & Cellular Biology, Tulane University, New Orleans, Louisiana, USA; [3]Department of Orthopaedic Surgery, Tulane University, New Orleans, Louisiana, USA; [4]Department of Pathology and Laboratory Medicine, Weill Cornell Medicine, New York, New York, USA; [5]Department of Pathology and Laboratory Medicine, Tulane University, New Orleans, Louisiana, USA; [6]Department of Biostatistics and Data Science, Tulane University, New Orleans, Louisiana, USA; [7]Tulane Cancer Center and Louisiana Cancer Research Consortium, Tulane University, New Orleans, Louisiana, USA; [8]Tulane Center for Stem Cell Research and Regenerative Medicine, Tulane University, New Orleans, Louisiana, USA; [9]Tulane Center for Aging, Tulane University, New Orleans, Louisiana, USA

*Correspondence: Zongbing.You@va.gov; zyou@tulane.edu; Tel.: +1-504-507-2000 Ext. 67364; +1-504-988-0467

All authors have no conflict of interest to declare.

Abstract

Interleukin-17 (IL-17) is a pro-inflammatory cytokine, participating in innate and adaptive immune responses, that plays an important role in host defense, autoimmune diseases, tissue regeneration, metabolic regulation, and tumor progression. Post-translational modifications (PTMs) are crucial for protein function, stability, cellular localization, cellular transduction, and cell death. However, PTMs of IL-17 receptor A (IL-17RA) have not been investigated. Here, we showed that human IL-17RA was targeted by F-box and WD repeats domain containing 11 (FBXW11) for ubiquitination, followed by proteasome-mediated degradation. We used bioinformatics tools and biochemical techniques to determine that FBXW11 ubiquitinated IL-17RA through a lysine 27-linked polyubiquitin chain, targeting IL-17RA for proteasomal degradation. Domain 665-804 of IL-17RA was critical for interaction with FBXW11 and subsequent ubiquitination. Our study demonstrates that FBXW11 regulates IL-17 signaling pathways at IL-17RA level.

Introduction

Cytokines of interleukin-17 (IL-17) family play various functions in innate and adaptive immune responses [1]. The IL-17 family consists of 6 members: IL-17A, IL-17B, IL-17C, IL-17D, IL-17E, and IL-17F. On the other hand, there are five canonical IL-17 receptors (IL-17Rs) interacting with them, including IL-17RA, IL-17RB, IL-17RC, IL-17RD, and IL-17RE [1]. Canonical IL-17Rs are unique because of their two conserved structural features: two extracellular fibronectin II-like domains and one intracellular domain named as similar expression to fibroblast growth factor genes and IL-17R (SEFIR) [2]. In addition to the canonical IL-17Rs, an uncanonical receptor CD93 was reported to be specifically expressed on the surface of group 3 innate lymphoid (ILC3) cells [3]. The ligand and receptor association between IL-17 cytokines and IL-17Rs is complex due to various binding forms. Among them, the most well-studied IL-17 cytokines are IL-17A and IL-17F, which share the highest structural conservation among the IL-17 cytokines [1]. IL-17A homodimer, IL-17F homodimer, and IL-17A/F heterodimer interact with IL-17RA/RC heterodimer or IL-17RC homodimer, inducing expression of various downstream genes [4]. IL-17RA heterodimerizes with IL-17RD, binding with IL-17A homodimer [5]. IL-17RA/RB heterodimer binds with IL-17E homodimer [6, 7]. IL-17RA also associates with IL-17RE to bind with IL-17C homodimer [8]. IL-17D was reported to bind CD93, regulating colonic inflammation [3]. Although IL-17B was originally considered as the ligand for IL-17RB, it is believed to be a competitor against IL-17E in binding to IL-17RB [9]. So far, IL-17RA is best-known as the common dimerization partner with all other canonical IL-17Rs, such as IL-17RC, IL-17RB, IL-17RD, and IL-17RE, indicating its unique functions in IL-17 signaling. Previous studies have delineated the special intracellular structures of IL-17RA beyond the SEFIR domain that are different from other canonical IL-17Rs [10, 11].

Ubiquitylation is one of the post-translational modifications (PTMs) of proteins, achieving quality control of cellular responses [12]. There are three main steps of ubiquitylation. Ubiquitin is first activated by adenosine triphosphate (ATP) and E1 enzyme. Then, the activated ubiquitin is conjugated to E2 enzyme. The last step is addition of a ubiquitin or polyubiquitin chains to a substrate by a particular E3 ligase [13]. There are more than 600 E3 ligases encoded by human genome, and they usually form a functional complex with other components [14]. Based on how ubiquitin is transferred to substrates and the core domain of the complex components that facilitates this process, E3 ligases are further classified into two major groups: homologous to E6-AP C terminus (HECT) domain-containing E3 ligases [15] (accounting for around 5% of E3 ligases [16]) and really interesting new genes (RING)-domain-containing E3 ligases [17] (accounting for around 95% of E3 ligases [16]). RING-domain-containing E3 ligases are further classified into RING domain variants, individual E3 ligases, anaphase promoting complex or cyclosome (APC/C) E3 ligases, and Cullin-Ring E3 ligases (CRL) which contain a scaffold protein Cullin [18]. CRL E3 ligase family constitutes more than 200 documented members, which is the largest class of E3 ligase family [19]. Based on different Cullins, CRL E3 ligase complex is further classified into 5 subfamilies (Cullin1, Cullin2/5, Cullin3, Cullin4A/4B, and Cullin7). Among them, the best known are the Skp1-Cullin1-F box protein (SCF) E3 ligases [16]. For CRL E3 ligases, before facilitating the transfer of ubiquitin to a substrate, they need to be activated by neddylation where neural-precursor-cell-expressed,

developmentally down-regulated gene 8 (NEDD8) interacts with Cullin [20]. After ubiquitylation, the outcome of the substrate is mostly dependent on which lysine is used for ubiquitylation. For lysine 48-linked polyubiquitylation, the substrate is usually subjected to proteasome-mediated degradation into small peptides. But for lysine 63-linked polyubiquitylation, the substrate is often activated to regulate signaling transduction and DNA repair [21]. The outcomes of the substrates varies when ubiquitin chains are formed using other lysine residues (K6, K11, K27, K29, and K33) or the first methionine residue (M1) [21].

The cascade of IL-17 signaling pathway initiates from the binding of IL-17A/IL-17F with IL-17RA/IL-17RC. After dimerized IL-17RA and IL-17RC recruit NF-κB activator 1 (Act1) through the SEFIR domain, activated Act1 further recruits and ubiquitylates tumor necrosis factor receptor associated factor 6 (TRAF6) by K63-linked polyubiquitin chain. Polyubiquitylated TRAF6 then activates transforming growth factor-beta-activated kinase 1 (TAK1), leading to activation of nuclear factor κB (NF-κB) and mitogen-activated protein kinase (MAPK) signaling pathways. Thereafter, IL-17-downsteam target genes, such as cytokines (tumor necrosis factor α, interleukin-1, and interleukin-6), chemokines (C-X-C motif ligand 1, C-X-C motif ligand 2, and C-C motif ligand 20), matrix metalloproteinases (MMP3, MMP7, and MMP9) start to be transcribed. On the other hand, to restrain IL-17 signaling, deubiquitinase A20 is upregulated upon IL-17 stimulation. Recruitment of A20 to IL-17RA through C/EBPβ activation domain (CBAD) performs a negative feedback to deubiquitylate TRAF6, restricting IL-17-dependent activation of NF-κB and MAPK signaling [22]. Besides, Act1 is ubiquitylated by beta-transducin repeat containing E3 ubiquitin protein ligase (bTrCP) through K48-linked polyubiquitin chain for proteasomal degradation after prolonged stimulation of IL-17 [23]. Phosphorylation of Act1 by TANK binding kinase 1 (TBK1) also suppresses IL-17-mediated activation of NF-κB in a TRAF6-dependent fashion [24].

Our previous study reported that IL-17RA is constitutively phosphorylated by glycogen synthase kinase 3 (GSK3) at threonine 780, leading to ubiquitylation and proteasomal degradation [25]. However, the specific E3 ligase mediating this process is still elusive. In the current study, we found that IL-17RA is ubiquitylated by SCF^{FBXW11} complex through K27-linked polyubiquitin. An intracellular 665-804 domain of IL-17RA is critical for ubiquitylation and degradation. Taking together with previous reports [23, 26], SCF^{FBXW11} complex not only regulates IL-17 signaling pathway at IL-17RA level, but also at Act1 and IκBα levels.

Results

Inhibition of proteasome and Cullin-Ring Ligase (CRL) complex increases IL-17RA protein stability. Our previous study reported that exogenous IL-17RA was degraded through a ubiquitin-proteasome system (UPS) [25]. But a specific E3 ligase mediating this process has not been identified. The CRL E3 ligase family contains the most diverse subunits with more than 200 E3 ligase members [16]. One of the core subunits of CRL E3 ligase complex is a scaffold protein Cullin. Neddylation of Cullin by interacting with NEDD8 activates E3 ligase complex to ubiquitylate the substrates [27]. To verify if IL-

17RA is degraded through proteasome and particularly by the CRL complex, full-length human IL-17RA was transiently overexpressed in HEK293T cells and then the cells were treated with cycloheximide (CHX). When protein synthesis was inhibited by CHX, total IL-17RA protein level decreased rapidly. A proteasome inhibitor MG132 and a neddylation inhibitor MLN4924 delayed degradation of exogenous IL-17RA (Figure 1A). Using the Human Protein Atlas (HPA) database, we examined mRNA levels of IL-17RA in different human cell lines and found that IL-17RA was ubiquitously expressed in human cell lines from different organs, although the expression levels were tremendously variable (Figure 1-figure supplement 1A). Because multiple commercially available anti-IL-17RA antibodies did not work well to detect endogenous IL-17RA, we used small interference RNA to knock down IL-17RA in HaCaT and 22Rv1 cell lines and probed with a G9 clone of monoclonal antibody obtained from Santa Cruz Biotechnology (cat# sc-376374, Dallas, TX). The results of Western blot analysis indicated that this G9 clone was able to specifically recognize endogenous IL-17RA (Figure 1-figure supplement 1B and C). Therefore, we used this antibody in our subsequent experiments to detect endogenous and exogenous IL-17RA.

Endogenous IL-17RA levels in 22Rv1 cells decreased rapidly after CHX treatment, while MG132 and MLN4924 inhibited this reduction (Figure 1B). This result was consistent with that of exogenous IL-17RA in HEK293T cells (Figure 1A). Treatment with MG132 also stabilized endogenous IL-17RA in HaCaT cells (Figure 1C). These findings indicate that degradation of exogenous and endogenous IL-17RA was mediated by a ubiquitin-proteasome system, particularly by the CRL complex as neddylation inhibitor delayed the degradation. We conducted further studies into the impact of neddylation inhibitor on endogenous IL-17RA levels in HaCaT, 22Rv1, and PC-3 cell lines using different dosages of MLN4924 over different time periods. As shown in Figure 1D-F, treatment with MLN4924 resulted in accumulation of endogenous IL-17RA and c-Myc, a well-known substrate ubiquitylated by a CRL E3 ligase F-box and WD repeat domain containing 7 (FBXW7) [28].

Bortezomib is another proteasome inhibitor that has been approved by the U.S. Food and Drug Administration (FDA) to treat multiple myeloma, mantle cell lymphoma, and acute allograft rejection [29]. HaCaT, THP-1, 22Rv1 and PC-3 cells were treated with different doses of bortezomib for 14 hours. The results showed that endogenous IL-17RA levels were slightly accumulated (Figure 1-figure supplement 2A-D). Combined treatment of CHX and bortezomib also showed that bortezomib slightly decreased degradation of endogenous IL-17RA (Figure 1-figure supplement 2E and F). It has been reported that bortezomib at a nano-molar concentration only inhibited ~70% activity of proteasome while MG132 at a micromolar concentration inhibited ~95% activity of proteasome [30], which explains why bortezomib only slightly prevented degradation of endogenous IL-17RA while MG132 dramatically prevented IL-17RA degradation. Besides proteasome-mediated degradation of damaged or misfolded proteins, autolysosomes also play a role to break down proteins through lysosomal enzymes [31]. To test if IL-17RA is also degraded through lysosomes, we treated HaCaT cells with different doses of lysosome inhibitor imidazole for different time periods. The results showed that alteration of IL-17RA

levels was not obvious, indicating that degradation of IL-17RA was probably not mediated through the lysosomes (Figure 1-figure supplement 2G and H).

F-box and WD repeat domain containing (FBXW) proteins are predicted to recognize IL-17RA. Having shown that IL-17RA was degraded by the ubiquitin-proteasome system, particularly through CRL complex, we investigated which E3 ligase targets IL-17RA for ubiquitylation and degradation. To narrow down our targets from more than 600 E3 ligases encoded by human genome [14], we first used bioinformatics tools to predict the potential candidates. We previously found that GSK3 phosphorylates IL-17RA at T780, leading to ubiquitylation and degradation of IL-17RA [25]. Therefore, we speculated that IL-17RA might have some phosphodegrons (short motifs with specific sequence pattern) that could be recognized by E3 ligases [32] for ubiquitylation and degradation [16]. In the protein sequence of human IL-17RA, there are two candidate phosphodegrons that can be recognized by FBXW7 and FBXW1A/FBXW11, which are conserved across different species (Figure 2-figure supplement 1A). FBXW proteins belong to CRL E3 ligases. Because Cullin1 and S-phase kinase associated protein 1 (Skp1) are required to form an E3 ligase complex, these CRL E3 ligases are called Skp1-Cullin1-F-box (SCF) E3 ligases [33]. In total, there are 10 members in the FBXW family, named from FBXW1A to FBXW12, except that FBXW3 is the pseudogene of FBXW4 and FBXW6 is identical to FBXW8 [34]. F-box domain and WD repeat domain are conserved across different FBXW E3 ligases (Figure 2-figure supplement 1B and C). Skp1 is an adaptor bridging F-box domain of FBXW E3 ligase and Cullin1 to form a complex. WD repeat domain is used to recognize a specific substrate for ubiquitylation [35]. Draberova, et al. applied mass spectrometry to analyze components in the precipitates pulled-down by recombinant Strep-Flag-tagged mouse IL-17A (SF-IL-17A). In addition to the well-known components of IL-17 signaling pathway that interact with IL-17, such as IL-17RA, IL-17RC, Act1 and TRAF6, they also found Cullin1 and beta-TrCP1/2 (also known as FBXW1A/11) [36], hinting at that FBXW1A and FBXW11 may physically bind to IL-17RA.

Several SCF E3 ligases are associated with IL-17RA. Because FBXW family members utilize the conserved WD domain to recognize substrates, we used co-immunoprecipitation (co-IP) assays to screen the FBXW proteins that might bind with IL-17RA. In HEK293T cells, Flag-tagged IL-17RA was co-transfected with Myc-tagged FBXW7 ΔF box, FBXW5, FBXW1A and Skp2. Our reciprocal co-IP results showed that FBXW7 ΔF box and FBXW5 had a strong association with IL-17RA, while FBXW1A had less binding with IL-17RA (Figure 2A). We also co-transfected Myc-His-tagged IL-17RA together with Flag-tagged FBXW2, FBXW4, FBXW8, FBXW9, FBXW11 and FBXW12. The co-IP results showed that the strongest binding partners of IL-17RA were FBXW9 and FBXW11 (Figure 2B). Because we used FBXW7 with truncation of F-box, we then used HA-tagged full-length FBXW7 to exam physical association and the results showed that FBXW7 weakly bound to IL-17RA (Figure 2-figure supplement 1D). Our co-IP data indicated that there are several E3 ligase candidates for IL-17RA, including FBXW1A, FBXW5, FBXW7, FBXW9 and FBXW11.

FBXW11 ubiquitylates IL-17RA via K27-linked polyubiquitin in a dose-dependent way. To determine which E3 ligase candidate has the highest activity to ubiquitylate IL-

17RA, Flag-tagged IL-17RA, HA-tagged wild-type (WT) ubiquitin and candidate E3 ligases were co-transfected into HEK293T cells and MG132 was used to treat the cells before extracting whole cell lysates. Anti-HA antibody was used to pull-down ubiquitylated substrates and anti-Flag and anti-IL-17RA antibodies were used to probe ubiquitylated IL-17RA. The ubiquitylation assays showed that FBXW11 had the highest activity to ubiquitylate IL-17RA, while FBXW9 and FBXW1A had much less activities than FBXW11 (Figure 3A). We also used Ni-NTA beads to pull down His-tagged ubiquitin and confirmed that FBXW11 had the highest activity to ubiquitylate IL-17RA (Figure 3-figure supplement 1A). Ubiquitylation of endogenous IL-17RA by FBXW11 in THP-1 and HCT116 cell lines was dose-dependent (Figure 3B and C). Engineered ubiquitin variants can selectively bind to ubiquitin-binding domains and block recognition of natural ubiquitylation substrates, thus they can be used to inhibit specific E3 ligase activity [37]. Ubv.Fw11.2 is such a ubiquitin variant selectively preventing formation of SCF^{FBXW11} complex [38]. We applied Ubv.Fw11.2 in our ubiquitylation assays and found that Ubv.Fw11.2 slightly inhibited ubiquitylation of endogenous IL-17RA in THP-1 cells but not in HCT116 cells (Figure 3B and C). A possible reason for this difference may be due to the low basal level of ubiquitylation present in these two cell lines.

It is known that seven lysine (K) residues and the first methionine (M) residue in the ubiquitin participate in forming ubiquitin chains. Of note, K11, K27 and K48 are involved in the proteasomal degradation of substrates [21]. In THP-1 and HCT116 cells, we co-transfected Flag-HA-FBXW11 along with His-tagged WT ubiquitin and a series of ubiquitin mutants with a single lysine-to-arginine substitution. The ubiquitylation assay results revealed that mutation of K27 into arginine (K27R) remarkably decreased ubiquitylation levels of IL-17RA in both cell lines, although mutation of other lysine residues also showed various degrees of reduction in ubiquitylation (Figure 3D and E). Besides, we also found that mutations of K48 and K63 slightly decreased ubiquitylation of IL-17RA in HCT116 cells (Figure 3E), which agreed with our previous report [25].

Overexpression of FBXW11 accelerates degradation of IL-17RA while knock-out of FBXW11 increases protein stability of IL-17RA. Having determined that FBXW11 is the E3 ligase involved in ubiquitylation of IL-17RA, we assessed the effects of FBXW11 on IL-17RA protein stability. Our lab previously established a HEK293 cell line named HEK293-IL-17RA that stably overexpresses Flag-IL-17RA [25]. We transfected Flag-FBXW4, Myc-FBXW5, Flag-HA-FBXW9, Myc-FBXW1A, or Flag-HA-FBXW11 into HEK293-IL-17RA cells and used CHX to inhibit protein synthesis. Western blot analysis showed that FBXW9 and FBXW11 dramatically accelerated degradation of Flag-IL-17RA (Figure 4A) compared to vector control and other E3 ligases. In THP-1 cells, ectopic overexpression of Myc-FBXW1A, Flag-HA-FBXW11, and Flag-HA-FBXW9 enhanced degradation of endogenous IL-17RA. In Ishikawa cell line, only FBXW11 remarkably accelerated degradation of endogenous IL-17RA (Figure 4B). These findings suggest that overexpression of FBXW11 decreased protein stability of IL-17RA. Next, we examined the effects of FBXW11 knock-out (KO) on IL-17RA protein stability. A549 FBXW11 KO cell line was generated using a clustered regularly interspaced short palindromic repeats (CRISPR)/CRISPR-associated protein 9 (Cas9) technique [39]. FBXW11 knock-out increased the basal levels of IL-17RA protein compared to the parental A549 FBXW11 WT cells. CHX treatment led to a rapid decrease of IL-17RA in FBXW11 WT cells but not

in FBXW11 KO cells (Figure 4C, left panel). It has been known that there is functional redundance between FBXW1A and FBXW11 [40]. FBXW1A siRNA was transiently delivered into both A549 FBXW11 WT and KO cells before treatment with CHX. It showed that knock-down of FBXW1A slightly stabilized endogenous IL-17RA compared to control siRNA group. To further verify our findings, we used CRISPR/Cas9 technique to knock out FBXW11 in Ishikawa cell line. Although basal level of endogenous IL-17RA protein was dramatically increased in Ishikawa FBXW11 KO cells compared to the parental WT cells, knock-down of FBXW1A didn't show any obvious effects on protein stability of endogenous IL-17RA (Figure 4C, right panel). These findings suggest that FBXW11 KO increases the protein stability of endogenous IL-17RA, while the effects of FBXW1A knock-down are dependent on the cellular context as shown in previous reports (comprehensively reviewed in [41]).

Expression levels of FBXW11 and IL-17RA are inversely correlated. Due to lack of good antibodies to detect endogenous FBXW11 (of note, we tested five different commercial antibodies, but none of them worked), we used real-time qPCR analysis to measure FBXW11 mRNA levels and Western blot analysis to quantify IL-17RA protein levels in 12 human cell lines (Figure 5A and B). Our results showed an inverse relationship between FBXW11 mRNA levels and IL-17RA protein levels, such that high FBXW11 mRNA levels were associated with low IL-17RA protein levels, and vice versa (Figure 5C). Pearson's correlation analysis showed that FBXW11 mRNA levels and IL-17RA protein levels were significantly inversely correlated (Figure 5D). We further explored a public protein database Clinical Proteomic Tumor Analysis Consortium (CPTAC) through the UALCAN platform (https://ualcan.path.uab.edu/analysis-prot.html) to analyze FBXW11 and IL-17RA protein levels across multiple cancer types. Our analysis showed that IL-17RA protein levels were significantly higher in brain tumors and uterine tumors than the corresponding normal control tissues. On the other hand, FBXW11 protein levels were significantly lower in brain tumors and uterine tumors than the corresponding normal control tissues (Figure 5E). Pearson's correlation analysis also revealed a significant inverse correlation between the protein levels of FBXW11 and IL-17RA in both the brain tissues (Figure 5F) and the uterine tissues (Figure 5G). Phosphorylation abundance of IL-17RA was analyzed using the LinkedOmicsKB platform (https://kb.linkedomics.org/) and found that the levels of IL-17RA phosphorylation at S629 and S708 in the uterine tumor samples were significantly lower than the corresponding normal controls (Figure 5-figure supplement 1A and B). The levels of IL-17RA phosphorylation at S801 in the uterine tumor samples were also lower than the corresponding normal controls, but there was no statistically significant difference likely due to the smaller sample size (Figure 5-figure supplement 1C). These findings are consistent with our hypothesis that phosphorylation accelerates IL-17RA degradation [25].

665-804 domain of IL-17RA determines its protein stability and ubiquitylation mediated by FBXW11. A previous report has shown that expression of IL-17RA Δ665 mutant was more robust than that of the full-length IL-17RA. Furthermore, treatment with TNF-α and IL-17A resulted in higher levels of IL-6 secretion in IL-17RA$^{-/-}$ fibroblasts expressing the IL-17RA Δ665 mutant compared to the cells expressing the full-length IL-17RA [10]. We generated two truncation mutants of human IL-17RA, including Flag-IL-

17RA Δ665-804 and Flag-IL-17RA Δ729-773 [25]. Not only are the putative candidate phosphodegrons located within the truncated 665-804 domain, but also there are multiple potential phosphorylation sites present within the domain (Figure 6A). Our co-IP assays revealed that deletion of amino acids 665-804 resulted in a remarkably lower binding association between truncated IL-17RA and FBXW1A or FBXW11, compared to the full-length IL-17RA. However, deletion of 729-773 didn't affect the physical binding compared to the full-length IL-17RA protein (Figure 6B). Our ubiquitylation assay results also showed that deletion of 665-804 domain dramatically decreased ubiquitylation of IL-17RA, compared to the full-length IL-17RA (Figure 6C). Ectopic overexpression of full-length IL-17RA and IL-17RA Δ665-804 in HEK293T cells revealed that protein levels of full-length IL-17RA dramatically decreased following treatment with CHX, whereas protein levels of IL-17RA Δ665-804 did not exhibit this trend (Figure 6D and E). Furthermore, treatment with MG132 significantly stabilized full-length IL-17RA protein but not IL-17RA Δ665-804 protein (Figure 6D and F).

Knock-out of FBXW11 suppresses expression of IL-17-downstream genes through inhibiting nuclear entry of NF-κB p65. Next, we investigated the functional effects of FBXW11 KO on IL-17 signaling pathways, including Akt, MAPK, and NF-κB. Our previous results showed that knock-out of FBXW11 led to a dramatic stabilization of IL-17RA protein in A549 cells and Ishikawa cells (Figure 4C). We treated A549 FBXW11 WT, A549 FBXW11 KO, Ishikawa FBXW11 WT, and Ishikawa FBXW11 KO cells with 20 ng/ml rhIL-17A for 10 and 30 minutes and examined the components of IL-17 signaling pathways using Western blot analysis. We found that rhIL-17A treatment dramatically increased the levels of phosphorylated p38 MAPK (p-p38 MAPK) in FBXW11 KO cells but not in FBXW11 WT cells (Figure 7A, Figure 7-figure supplement 1A). The levels of phosphorylated ERK1/2 (p-ERK1/2) were higher in FBXW11 KO cells than those in FBXW11 WT cells after rhIL-17A treatment (Figure 7B, Figure 7-figure supplement 1B). Treatment with rhIL-17A did not increase levels of phosphorylated Akt (p-AKT) in either A549 or Ishikawa cell lines. Phosphorylated JNK (p-JNK) was obviously induced after 30-minutes treatment in Ishikawa cells but not in A549 cells (Figure 7B, Figure 7-figure supplement 1B). The basal levels of phosphorylated IκBα (p-IκBα) in FBXW11 KO cells were higher than those in FBXW11 WT cells, and treatment with rhIL-17A for 10 and 30 minutes also induced more p-IκBα in FBXW11 KO cells compared to FBXW11 WT cells. Correspondingly, a decrease of IκBα levels was observed in both FBXW11 WT and KO cell lines, but the levels of IκBα in FBXW11 KO cells were not less than those in FBXW11 WT cells after rhIL-17A treatment (Figure 7C, Figure 7-figure supplement 1C). Moreover, in our cell fractionation experiments, we observed that the nuclear protein levels of NF-κB p65 in FBXW11 KO cells were obviously lower than those in FBXW11 WT cells, both at the basal levels and after rhIL-17A treatment. However, the cytoplasmic NF-κB p65 levels in both WT and KO cell lines were almost equal, regardless of rhIL-17A treatment (Figure 7D). These results suggest that knock-out of FBXW11 prevents nuclear entry of NF-κB p65. It is well-known that E3 ligases FBXW1A/FBXW11 mediate ubiquitylation and degradation of p-IκBα [26]. In our A549 FBXW11 KO cells, knock-out of FBXW11

increased the basal levels of IκBα (Figure 7C) as ubiquitylation of IκBα was reduced due to lack of FBXW11. Therefore, IκBα continued to bind to and keep NF-κB p65/p50 in the cytoplasm. Even after rhIL-17A treatment, nuclear entry of NF-κB p65 in A549 FBXW11 KO cells was much less than that in A549 FBXW11 WT cells (Figure 7D), resulting in reduced transcriptional activities of NF-κB. Since NF-κB is the main transcription factor that initiates expression of IL-17-downstream genes, we predicted that IL-17 cytokines might fail to induce expression of IL-17-downstream genes in FBXW11 KO cells. To verify our prediction, we applied real-time qPCR assays to analyze expression of IL-17-downstream genes. Since IL-17RA is a common subunit dimerizing with other IL-17Rs to interact with different IL-17 cytokines (IL-17A, IL-17B, IL-17C, IL-17E, and IL-17F), we treated A549 FBXW11 WT and A549 FBXW11 KO cells with 20 ng/ml rhIL-17A, rhIL-17B, rhIL-17C, rhIL-17E, and rhIL-17F for 2 hours, individually. Treatment with rhIL-17A significantly increased expression levels of CXCL1 (Figure 7E), CXCL2 (Figure 7F), CXCL8 (Figure 7G), and IL-6 (Figure 7I) in A549 FBXW11 WT cells, while other IL-17 cytokines only significantly increased the levels of IL-6 expression (Figure 7I). As predicted, we observed that knock-out of FBXW11 significantly decreased the expression levels of IL-17-downstream genes upon treatment with IL-17 cytokines (Figure 7E-I). Real-time qPCR analysis of the same IL-17-downstream genes in Ishikawa FBXW11 WT and FBXW KO cell lines showed similar results (Figure 7-figure supplement 1D-H).

Discussion

IL-17-mediated inflammation is critical for innate and adaptive immune responses. Various interaction forms between IL-17 cytokines and receptors have attracted researchers to deepen their understanding of expression patterns, localization, and roles of each single IL-17 cytokine and receptor under different conditions [1, 9, 42]. In addition, most of the research activities have been focused on modulation of downstream signaling pathways of IL-17 receptor and their roles in physiological and pathological situations [43-46]. PTMs of proteins, such as phosphorylation and ubiquitylation, play significant roles in protein quality control, protein activity, gene expression, inter-/intra-cellular communications, and cellular activities [12, 47-49]. However, seldom studies have investigated PTMs of IL-17 receptors. To our best knowledge, our group first reported that IL-17RA was constitutively phosphorylated by GSK3 at threonine 780 (T780), leading to ubiquitylation and degradation, and IL-17RA phosphorylation was reduced in prostate cancer tissues compared to normal control tissues [25]. However, the specific E3 ligase mediating ubiquitylation of IL-17RA has not been identified. Another group reported that ubiquitylation of IL-17RA by TRAF6 upon IL-17F stimulation is required for downstream signaling [50]. In the current study, we determined that SCF^{FBXW11} complex mediated ubiquitylation of IL-17RA through recognizing 665-804 domain of IL-17RA.

We first used MG132 and MLN4924 treatment to verify that degradation of exogenous and endogenous IL-17RA was mediated by the proteasome, particularly by Cullin-Ring E3 ligase (CRL) complex (Figure 1A-F). In addition, we used an FDA-approved proteasome inhibitor bortezomib to further confirm that degradation of endogenous IL-

17RA was mediated by the proteasome (Figure 1-figure supplement 2A-F). Lysosome inhibitor imidazole was used to exclude the possibility of lysosome-mediated degradation of IL-17RA (Figure 1-figure supplement 2G and H).

More than 600 E3 ligases are encoded by human genome and more than 200 of them belong to the CRL E3 ligase family [16]. To narrow down the numbers of E3 ligase candidates targeting IL-17RA for ubiquitylation, we carried out phosphodegron predictions. Phosphodegron is a short linear motif that can be recognized by E3 ligases after phosphorylation. FBXW7 mediates ubiquitylation and degradation of multiple oncogenes, such as c-Myc and c-Jun [28, 51, 52]. In our prediction, a short linear motif (780-TPYEEE-785) of human IL-17RA matched with a phosphodegron TPxxE, which is recognized by FBXW7 (Figure 2-figure supplement 1A) [53]. On the other hand, another short linear motif (725-DSPLGSST-732) of human IL-17RA also matched with a phosphodegron DSGxxST, which is recognized by FBXW1A/FBXW11 (Figure 2-figure supplement 1A) [40]. The roles of FBXW1A/FBXW11 are context dependent, and FBXW1A and FBXW11 are believed to be functionally redundant [54]. When IL-17-binding proteins were precipitated by IL-17A cytokine, E3 ligases FBXW1A/FBXW11 and scaffold protein Cullin1 were among the components of IL-17-binding proteins [36, 55]. In addition, IL-17RA was listed among thousands of candidate substrates that might bind with FBXW11 using a parallel adaptor capture proteomics (PAC) approach (see Table S1 of [56]), but IL-17RA was not ranked high enough to be considered as an FBXW11 substrate by the investigators. Based on our phosphodegron predictions and the published hints, we hypothesized that FBXW7, FBXW1A, and FBXW11 might be the candidate E3 ligases. These three E3 ligases belong to FBXW family with 10 members that interact with phosphodegrons of a specific substrate through the WD repeat domain [33]. To determine which specific FBXW family member binds to IL-17RA, we performed co-IP assays and showed that FBXW1A, FBXW5, FBXW7, FBXW9, and FBXW11 had the highest binding association towards IL-17RA (Figure 2A and B). Since the WD repeat domain is a conserved domain and percent identity analysis showed that FBXW1A, FBXW7, and FBXW11 bear the greatest sequence similarities (Figure 2-figure supplement 1B and C), it is reasonable that multiple FBXW family members showed various degrees of binding to IL-17RA. Another possible reason could be that our co-IP assays were conducted in an overexpressed system and non-specific binding could not be completely avoided. Since the functions of SCF E3 ligases are to ubiquitylate the substrates, we performed ubiquitylation assays using two different approaches and both consistently demonstrated that FBXW11 had the highest E3 ligase activity among the candidates (Figure 3A, Figure 3-figure supplement 1A). Furthermore, we confirmed that FBXW11-mediated ubiquitylation of IL-17RA was dose-dependent (Figure 3B and C), implying that the ubiquitylation activity of FBXW11 towards IL-17RA is specific. Further, engineered ubiquitin variant Ubv.Fw11.2 slightly decreased basal ubiquitylation levels of endogenous IL-17RA by FBXW11 in THP-1 cells (Figure 3B). Taken together, our findings suggest that FBXW11 is the specific E3 ligase that ubiquitylates IL-17RA.

It has been well-documented that K48-linked polyubiquitin participates in proteasomal degradation of proteins and K63-linked polyubiquitin is involved in activation of protein and signaling transduction [57-59]. We found that single K27R mutation of the ubiquitin

remarkably decreased ubiquitylation levels of endogenous IL-17RA in both THP-1 and HCT116 cell lines, although a single mutation of other lysine residues also showed various degrees of reduced ubiquitylation (Figure 3D and E). These findings suggest that K27 is critical for FBXW11-mediated ubiquitylation of IL-17RA. It is possible that other lysine linked-polyubiquitin chains are secondary to K27-linked polyubiquitin. Since mixed-ubiquitylation-dependent regulation of protein stability has been documented [58, 60, 61], we cannot exclude the possibility that FBXW11 ubiquitylates IL-17RA through mixed-polyubiquitin chains. Beyond K48- and K63-linked polyubiquitination, polyubiquitination mediated by other lysine residues is termed as non-canonic ubiquitylation and they are poorly understood so far [59]. K27-linked non-canonic ubiquitylation is indispensable in immune response, cytokines signaling, T cell activation and differentiation [21]. IL-17RA is a key receptor in the IL-17 signaling and Th17 inflammatory responses, therefore our discovery further demonstrates the importance of K27-linked polyubiquitylation in the immune systems.

We found that overexpression of FBXW11 accelerated degradation of IL-17RA (Figure 4A and B) while knock-out of FBXW11 increased protein stability of IL-17RA (Figure 4C). Although knock-out of FBXW11 didn't completely block the degradation of IL-17RA, which was attributed to FBXW1A compensation in A549 cell line but not in Ishikawa cell line [62]. We demonstrated an inverse correlation between FBXW11 mRNA levels and IL-17RA protein levels in 12 human cell lines, including immortalized normal cell lines and cancer cell lines (Figure 5A-D). Further exploration of public proteomics database also showed that FBXW11 protein levels were inversely correlated with IL-17RA protein levels in the brain and uterine tissues (Figure 5E-G). These results suggest that FBXW11 downregulates IL-17RA protein levels in both human cell lines and human tissues.

Intracellular domain of IL-17RA beyond SEFIR domain has been shown to be critical for IL-6 secretion after stimulating with IL-17 and TNFα and the protein levels of IL-17RA Δ665 truncation mutant was robustly higher than full-length IL-17RA [10]. We generated two truncation mutants (IL-17RA Δ729-773 and IL-17RA Δ665-804) and demonstrated that deletion of Δ665-804 not only reduced binding with FBXW1A and FBXW11, but also decreased ubiquitylation mediated by FBXW11 (Figure 6A-C). Further, IL-17RA Δ665-804 truncation mutant was more stable than the full-length IL-17RA (Figure 6D-F). These findings indicate that 665-804 domain is critical for ubiquitylation and degradation of IL-17RA. However, we didn't examine which amino acid residue of IL-17RA is responsible for phosphorylation and subsequent ubiquitylation in the present study, which remains to be determined in future studies. Ubiquitylation is largely dependent on priming phosphorylation of the substrates [28, 63] and we predicted a candidate phosphodegron recognized by FBXW1A and FBXW11 together with multiple potential phosphorylation sites in the 665-804 domain. We believe that phosphorylation-dependent ubiquitylation of IL-17RA happens within this domain. The levels of IL-17RA phosphorylation at S708 and S801 in the uterine tumor samples were significantly lower than the corresponding normal controls (Figure 5-figure supplement 1A-C), while the levels of IL-17RA protein were higher in the uterine tumors than the normal tissues, suggesting that reduced IL-17RA phosphorylation is linked to more stable IL-17RA protein due to less ubiquitylation and degradation. Further study is needed to illustrate the specific amino acids of IL-17RA that

are involved in phosphorylation and ubiquitylation, which could be explored as therapeutic targets using proteolysis-targeting chimera (PROTAC) technique in the treatment of autoimmunity and cancer [64].

Since knock-out of FBXW11 remarkably increased endogenous IL-17RA protein levels in A549 and Ishikawa cell lines, we hypothesized that IL-17 cytokines that interact with IL-17RA should activate IL-17 signaling pathways, inducing higher levels of expression of downstream genes in FBXW11 KO cells, compared to the parental FBXW11 WT cells. However, we found that nuclear levels of NF-κB p65 in FBXW11 KO cells were much less than FBXW11 WT cells after 30-minutes treatment with rhIL-17A (Figure 7D). This raised a question why nuclear entry of NF-κB p65 was decreased in FBXW11 KO cells. Normally, IL-17 signaling is initiated by IL-17A binding to the receptors, leading to phosphorylation of IκBα. Phosphorylated IκBα is ubiquitylated by FBXW1A/FBXW11, resulting in proteasome-mediated degradation [26]. Degradation of IκBα liberates NF-κB p50/p65 to enter the nucleus, thus starting transcription of downstream genes [1, 65]. Yet, FBXW11 knockout led to a failure in ubiquitylation and degradation of IκBα, allowing IκBα to continue to trap NF-κB p50/p65 in the cytoplasm and subsequently fail to initiate expression of downstream genes. Furthermore, our real-time qPCR analysis confirmed the lower levels of basal and induced expression of downstream genes in FBXW11 KO cells compared to FBXW11WT cells (Figure 7E-I, Figure 7-figure supplement 1D-H). In addition, as a core component of IL-17 signaling, Act1 has been shown to be ubiquitylated by FBXW1A/FBXW11 and degraded by the proteasome [23]. Overall, IL-17 signaling is finely regulated by FBXW1A/FBXW11 at different levels, including IL-17RA, Act1, and IκBα (Figure 8). The present study found that IL-17RA was ubiquitylated by FBXW11, followed by proteasomal degradation. Knock-out of FBXW11 stabilizes IL-17RA and Act1, which is supposed to enhance IL-17 signaling and induce more expression of downstream genes. However, knock-out of FBXW11 decreases degradation of IκBα. Therefore, the end readouts of IL-17 signaling, that is, the expression levels of downstream genes, are reduced in FBXW11 KO cells. Treatment with rIL-17A induced more activation of MAPK signaling pathways in FBXW11 KO cells than WT cells, but the MAPK signaling pathways might not be involved in the expression of the IL-17-downstream genes examined. The biological significance of MAPK activation in this setting remains unknown, which should be investigated in future studies.

In summary, the present study identified SCF^{FBXW11} as a critical E3 ligase that regulates IL-17 signaling pathway at IL-17RA level. Future studies may be conducted to explore the potential of targeting SCF^{FBXW11} for the treatment of IL-17-dependent inflammatory and autoimmune conditions as well as cancers.

Materials and Methods

Mammalian cell culture. Human prostate cancer cell lines 22Rv1, PC-3 and LNCaP, human normal keratinocyte HaCaT, human embryonic kidney cell line HEK293T, human cervical cancer cell line HeLa, human lung cancer cell line A549, and human monocytic leukemia cell line THP-1 were purchased from the American Type Culture Collection (ATCC, Manassas, VA, U.S.A.). Human skin squamous cell carcinoma cell line A-431

was kindly gifted by Dr. Shitao Li at Tulane University. Human endometrial cancer cell line Ishikawa was kindly gifted by Dr. Matthew Burow at Tulane University. Human colon cancer cell lines HCT116 and DLD1 were kindly gifted by Dr. Lin Zhang at the University of Pittsburgh. Stable cell line HEK293-IL-17RA overexpressing exogenous Flag-IL-17RA was established in Dr. You's lab [25]. A549 FBXW11 WT and FBXW11 KO cell lines were kindly gifted by Dr. Friedemann Weber at Institute for Virology, FB10-Veterinary Medicine, Justus-Liebig University, with the permission of Dr. Veit Hornung at Ludwig-Maximilians-Universität Munich [39]. HaCaT, HEK293T, HeLa, A549, A-431, Ishikawa, HCT116, DLD1, HEK293-IL17RA, A549 FBXW11 WT, and A549 FBXW11 KO cell lines were maintained in high-glucose Dulbecco's Modified Eagle Medium (DMEM) Genesee (Scientific, San Diego, CA, U.S.A., #25-500) supplied with 10% fetal bovine serum (FBS, ATCC, Manassas, VA, U.S.A., #30-2022). THP-1, 22Rv1, and LNCaP cell lines were maintained in RPMI-1640 (Genesee Scientific, San Diego, CA, U.S.A., #25-506) medium supplied with 10% FBS. PC-3 cell line was maintained in Kaighn's Modification of Ham's F-12 (F-12K) (ATCC, #30-2004) supplied with 10% FBS. All cell lines were maintained in a humidified condition at 37 °C with 5% carbon dioxide. Where indicated, cells were treated with cycloheximide (CHX, Millipore Sigma, #01810), MG132 (Millipore Sigma, #M8699; Cayman chemical company, #10012628), bortezomib (Selleckchem, #S1013), MLN4924 (Selleckchem, #S7109), and imidazole (Fisher scientific, #A10221.36) dissolved in dimethyl sulfoxide (DMSO) (Fisher scientific, #BP231-100).

Plasmids. The following plasmids were purchased from Addgene: HA-Ubiquitin WT (#17608), Myc-FBXW7 ΔF box (#16652), Myc-FBXW5 (#19905), Myc-FBXW1A (#20718), and Myc-Skp2 (#19947). The following plasmids were kindly gifted by Dr. Michael Pagano at New York University: Flag-FBXW2, Flag-FBXW4, Flag-HA-FBXW8, Flag-HA-FBXW9, Flag-HA-FBXW11, and Flag-HA-FBXW12. The following plasmids were kindly gifted by Dr. Hua Lu at Tulane University: His-ubiquitin WT, His-ubiquitin K6R, His-ubiquitin K11R, His-ubiquitin K27R, His-ubiquitin K29R, His-ubiquitin K33R, His-ubiquitin K48R, and His-ubiquitin K63R [66]. Plasmids of lentiCRISPRv2 (addgene, #52961), pMD2.G (addgene, #12259) and psPAX2 (addgene, #12260) were also kindly gifted by Dr. Hua Lu at Tulane University. Flag-IL-17RA full-length plasmid was obtained from Dr. Xiaoxia Li [67] and it was used as a template to create Flag-IL-17RA Δ729-773 and Flag-IL-17RA Δ665-804 truncation mutants. Myc-His-IL-17RA plasmid was generated as previously described [68].

CRSIPR/Cas9-mediated gene knock-out. Targeting exon sequence (5'-GTGGACGACACAACTTGCAGAGG-3') was selected by the CHOPCHOP online tool (http://chopchop.cbu.uib.no/) and this target was validated by Dr. Friedemann Weber and Dr. Veit Hornung [39]. Standard de-salted oligos (Oligo 1: 5'-CACCG**GTGGACGACACAAC TTGCAG**-3', Oligo 2: 3'-C**CACCTGCTGTGTTGAACGTC**CAAA-5') were synthesized by Eurofins Genomics and were diluted to 100 μM in sterile water. GeCKO system was applied to generate lentiviral CRISPR tool following well-established protocols from Dr. Feng Zhang's lab [69, 70]. Oligo 1 and oligo 2 were annealed by T4 polynucleotide kinase (NEB, #M0201S) at 37 ℃ for 30 min and 95 ℃ for 5 min, then the temperature ramped down

to 25 ℃ at 5 ℃/min. The lentiCRISPRv2 was digested by BsmBI-v2 (NEB, #R0739S) at 55 ℃ for 15 min and heated to be inactivated at 80 ℃ for 20 min before chilling on ice. Digested lentiCRISPRv2 and annealed oligos were ligated with T4 DNA ligase (NEB, #M0202S) at 16 ℃ overnight and were heated to be inactivated at 65 ℃ for 10 min before chilling on ice. 5 µl of ligation product was transformed into 50 µl of Stbl3 competent cells (Invitrogen, #C737303). Insertion of guide RNA into lentiviral CRISPR plasmid was verified by Sanger sequencing under U6-forward primer (5'-GACTATCATATGCTTACCGT-3') before packaging lentiviruses. HEK293T cells were placed into a 10-cm dish 24 hours before transfection, supplied with 7 ml of Dulbecco's Modified Eagle's Medium (Genesee, #25-500) containing 10% fetal bovine serum. When the confluency reached 70-80%, jetPRIME (Polyplus, #101000046) was used to carry out co-transfection according to manufacturer's instructions. The amount of each plasmid was 5 µg recombinant lentiCRISPR, 2 µg pMD2.G, and 3 µg psPAX2. Plasmids were incubated for 12 hours before replacing with 6 ml of fresh complete culture medium. The supernatant containing lentiviruses was collected two times at 48 hours and 96 hours post-transfection. The supernatant containing lentiviruses was centrifuged at 1,000 rpm for 5 min at room temperature and aliquoted to be stored at -80 ℃. 24 hours before infecting with lentiviruses containing guide RNA targeting FBXW11 or empty vector, Ishikawa cells were seeded into a well of 6-well plate. When the cell confluency reached 30-50%, a mixture of 500 µl of fresh culture medium, 500 µl of virus medium, and 8 µg/ml of polybrene was added into the cells. 24 hours post the first infection, the infection was repeated once. 48 hours post the second infection, 1 µg/ul puromycin was used to select cells with successful infection. 7 days later, the surviving cells were serially diluted and placed into 96-well plates at a density of 0.5 cell per well. Puromycin selection was maintained for another 3-4 weeks until colonies were visible by naked eyes. Colonies were picked up to amplify before isolating genomic DNA using Quick-DNA miniprep Plus kit (Zymo research, #D4068). Standard PCR with a forward primer (5'-TATCGGTGGTATGCTGTTTCTG-3') and a reverse primer (5'-TCTCGTAGGCCAC TGATAATTT-3') was applied to amplify the target DNA sequence. Sanger sequencing was used to determine genotype of clones with the PCR primers. One clone (termed C1) that contained a 4-base pair deletion at the target site (5'-GTGGACGACACAA**----**CAGAGG-3') was selected as the FBXW11 knock-out cell line.

Transfection of plasmids and small interference RNA (siRNA). Human IL-17RA siRNA (#sc-40037) and nontargeting control RNA (#sc-37007) were obtained from Santa Cruz Biotechnology. Human FBXW1A siRNAs (#D-003463-01-0002, D-003463-02-0002, D-003463-03-0002, and D-003463-04-0002) were purchased from Dharmacon. AllStars Negative Control RNA (#SI03650318) was obtained from QIAGEN. Cells were transfected with plasmids or siRNA when the confluency reached around 70-80%. Transfection was performed using jetPRIME transfection reagent (Polyplus, #114-15) according to manufacturer's instructions. After transfection, the cells were incubated for 12-24 hours before replacing with fresh culture medium and subsequent treatments were conducted appropriately.

Western blot analysis. Cells were washed with phosphate buffered saline (PBS) and lysed with radioimmunoprecipitation assay (RIPA) buffer (50 mM sodium fluoride, 0.5% NP-40, 10 mM sodium phosphate monobasic, 150 mM sodium chloride, 25 mM Tris pH 8.0, 2 mM ethylenediaminetetraacetic (EDTA), and 0.2 mM sodium vanadate) with a fresh supplement of 1× protease inhibitor cocktail (PIC, Millipore Sigma, #P8849). After incubation on ice for 15 min, cell lysate was centrifuged at 13,000 *x g* for 15 min at 4 ℃. The supernatant of whole cell lysate was transferred into a new microcentrifuge tube and boiled with 3x sample loading buffer (208.1 mM sodium dodecyl sulfate (SDS), 30% glycerol, 187.5 mM Tris pH 6.8, 15% β-mercaptoethanol, 14.9 mM bromophenol blue) at 100 ℃ for 5-10 min. Around 60-120 µg of total protein was subject to sodium dodecyl sulfate polyacrylamide gel electrophoresis (SDS-PAGE) and transblotted to the polyvinylidene fluoride membranes (PVDF, Genesee Scientific, #83-646R). The blots were blocked with 2.5% bovine serum albumin (Millipore Sigma, #A3294) solution containing 0.02% sodium azide (Millipore Sigma, #S2002). The blots were probed with the following primary antibodies at room temperature for 1-2 hours or at 4 ℃ overnight: anti-GAPDH (Millipore, #MAB374, 1:5,000 dilution), anti-Flag M2 (Sigma, #F3165, 1:20,000 dilution), anti-IL-17RA (Santa Cruz Biotechnology, #sc-376374, 1:500 dilution), anti-c-Myc (Santa Cruz Biotechnology, #sc-40, 1:1,000 dilution), anti-c-Myc (Novus, #NB600-335, 1:1,000 dilution), anti-HA (Santa Cruz Biotechnology, #sc-7392, 1:1,000 dilution), anti-FBXW7 (Bethyl Laboratories, #A301-720A, 1:15,000 dilution), anti-p-Akt (Cell Signaling Technology, #9271, 1:500 dilution), anti-Akt (Santa Cruz Biotechnology, #sc-81434, 1:100 dilution), anti-p-IκBα (Cell Signaling Technology, #2859, 1:1,000 dilution), anti-IκBα (Cell Signaling Technology, #4814, 1:1,000 dilution), anti-p-JNK (Cell Signaling Technology, #9255, 1:500 dilution), anti-JNK (Cell Signaling Technology, #9252, 1:1,000 dilution), anti-p-ERK1/2 (Santa Cruz Biotechnology, #sc-7383, 1:500 dilution), anti-ERK1/2 (Cell Signaling Technology, #4695, 1:1,000 dilution), anti-p-p38 MAPK (Santa Cruz Biotechnology, #sc-166182, 1:500 dilution), anti-p38 MAPK (Cell Signaling Technology, #8690, 1:1,000 dilution), anti-NF-κB p65 (Cell Signaling Technology, #6956, 1:500 dilution), anti-β-tubulin (Cell Signaling Technology, #2128, 1:1,000 dilution), and anti-Histone H3 (Cell Signaling Technology, #4499, 1:2,000 dilution). Li-Cor IRDye680- and IRDye800-conjugated secondary antibodies were incubated at room temperature for 45 min at a dilution of 1: 10,000 and 1: 5,000, respectively. The blots were scanned with a Li-COR Odyssey 9120 Digital Imaging system. When necessary, the blots were stripped with a stripping buffer (62 mM Tris-HCl pH 6.7, 2% SDS, and 100 mM β-mercaptoethanol) and re-scanned to confirm stripping efficiency before probing for another antigen of interest. Adobe illustrator was utilized to organize images.

Co-immunoprecipitation (co-IP). HEK293T cells were seeded at a density of 1x10^6 cells per 6-cm dish or 4.5x10^6 cells per 10-cm dish, approximately 20 hours prior to transfection. 3 ml and 7 ml of DMEM (with 10% FBS) were added to the 6-cm and 10-cm dishes, respectively. Transient transfection of plasmids was conducted using jetPRIME (Polyplus, #114) according to the manufacturer's instructions. 48 hours post transfection, protein was extracted with an IP lysis buffer (50 mM Tris-HCl pH 7.5, 0.5% Nonidet P-40, 1 mM EDTA, and 150 mM NaCl). IP lysis buffer was freshly supplemented with 1x PIC and 1 mM 1,4-dithiothreitol (DTT, Thermo Fisher, #R0861). A proper amount of lysis buffer was added and vortexed vigorously for 10 sec, followed by incubation on ice for 30 min

and vortexing every 10 min. Cell debris was removed by centrifuging at 13,000 *x g* at 4 ℃ for 15 min. Supernatant was transferred into a new centrifuge tube and protein concentration was quantified with Bradford assay [71]. Immunoprecipitation was carried out by mixing 500-800 μg of whole cell lysate and 1-2 μg of anti-Flag M2 antibody (Sigma Millipore, #F3165), 1-2 μg of anti-c-Myc antibody (Santa Cruz Biotechnology, #sc-40), or 12 μg of anti-FBXW7 antibody (Bethyl Laboratories, #A301-720A). 1-2 hours later, 20 μl of 75% (v/v) rProtein A agarose resin beads (Genesee Scientific, #20-525) were added into each sample and kept incubation with gentle rocking at 4℃ overnight. The beads were washed with 1 ml of pre-chilled IP lysis buffer (freshly supplemented with 1 mM DTT and 1x PIC) 3 times. The precipitated proteins were eluted in 20 μl of 2x sample loading buffer with boiling at 100 ℃ for 5 min. Samples were subject to Western blot analysis.

Ubiquitylation assay. 42 hours post-transfection, cells were treated with 20 μM MG132 for 6–8 hours. The cells were collected and washed with PBS once. When Ni-NTA resins (Thermo Fisher, #88221) were used, the cell pellet was aliquoted into two parts: 25% of the cells was lysed with RIPA buffer, freshly supplemented with 1 x PIC, on ice for 10 min and 75% of cells was lysed with fresh Buffer B (8 M Urea, 0.1 M Na_2HPO_4/NaH_2PO_4, pH 8.0, 0.01 M Tris-Cl pH 8.0, 10 mM β-mecaptoethanol, and 25 mM imidazole) at room temperature for 10 min. The supernatant was collected after centrifuge at 13,000 *x g* for 15 min at 4℃ or room temperature, respectively. The whole cell lysate extracted with RIPA buffer was subject to SDS-PAGE and the signal intensity of IL-17RA detected with Western blot was used to adjust the amount of cell lysate of each sample applied to subsequent pull-down assays, in order to keep equal amount of proteins used for each pull-down reaction. 30 μl of 50% Ni-NTA resins was washed three times with Buffer B and then resuspended in 100 μl of Buffer B. The resins were incubated with proper volume of cell lysate extracted with Buffer B at room temperature for 4 hours. The Ni-NTA resins were washed with 1 ml of Buffer B 3 times and 1 ml of fresh Buffer C (8 M Urea, 0.1 M Na_2HPO_4/NaH_2PO_4, pH 6.3, 0.01 M Tris-Cl pH 6.3, and 10 mM β-mecaptoethanol) for 2 times. The samples were processed for elution with boiling twice in 1x sample loading buffer containing 300 mM imidazole at 100 ℃ for 3 min each time. When rProtein A agarose resins were used, the cell pellet was boiled in 120 μl of denaturing IP lysis buffer (50 mM Tris-HCl pH 7.5, 0.5% Nonidet P-40, 1 mM EDTA, 150 mM NaCl, freshly supplemented with 1x PIC, 1 mM DTT, and 1% SDS) at 100℃ for 10 min. After centrifuging at 13,000 *x g* at room temperature for 15 min, 110 μl of supernatant was collected. 20 μl of supernatant was aliquoted into a new tube as whole cell lysate sample and boiled with 3x sample loading buffer for 5 min. The rest of 90 μl supernatant was diluted with freshly prepared IP lysis buffer (without SDS) until the concentration of SDS was less than 0.1%. Before immunoprecipitation, a direct Western blot analysis was conducted to decide the proper amount of cell lysate needed. During immunoprecipitation, 3 μg anti-HA antibody (Santa Cruz Biotechnology, #sc-7392) was used to pull down ubiquitin-conjugated IL-17RA, which was incubated at 4℃ with gentle agitation for 1-2 hours. Then, 20 μl of 75%(v/v) rProtein A agarose resins were added into each sample. Samples were incubated with gentle rocking at 4℃ overnight. The resin beads were washed with 1 ml pre-chilled IP lysis buffer (freshly supplemented with 1 mM DTT and 1 x PIC) for 3 times and boiled with 20 μl 2x loading buffer at 100℃ to elute the precipitated

proteins, which was repeated once to achieve a thorough elution. Samples were subjected to subsequent Western blot analysis.

Nuclear and cytoplasmic protein extraction. For both A549 and Ishikawa cell lines, 24 hours before treatment, 2.0 x 10^6 FBXW11 WT and 2.5 x 10^6 FBXW11 KO cells were seeded into 10-cm dishes. 20 ng/ml recombinant human IL-17A (rhIL-17A, R&D Systems, #7955-IL-025/CF) was used to treat the cells for 10 or 30 minutes. According to manufacturer's instructions, cytoplasmic and nuclear proteins were extracted using NE-PER nuclear and cytoplasmic extraction kit (Thermo Scientific, #78833). In brief, FBXW11 WT and FBXW11 KO cells were collected with trypsin-EDTA. After centrifuge at 500 x *g* for 5 minutes at 4 ℃, the supernatant was discarded. 200 µl ice-cold cell extraction reagent I was added and vortexed vigorously for 15 seconds to lyse cell membrane, followed by incubation for 10 minutes and adding 11 µl ice-cold cell extraction reagent II. The lysates were vortexed for 5 minutes and incubated on ice for 1 min. The supernatant was transferred into a new tube after centrifuging at 13,000 x *g* for 15 minutes. The insoluble pellet was resuspended with 50-100 µl nuclear extraction reagent and vortexed for 15 seconds, followed by incubation on ice for 40 minutes with vortexing every 10 minutes. The supernatant was collected after centrifuging at 13,000 x *g* for 15 minutes. The protein concentration was quantified with a Take3 microplate spectrometer (BioTeck, Synergy H1).

Quantitative real-time PCR (qPCR) analysis. FBXW11 WT and FBXW11 KO cell lines (A549 and Ishikawa) were treated with 20 ng/ml rhIL-17A (R&D Systems, #7955-IL-025/CF), rhIL-17B (R&D Systems, #8129-IL-025/CF), rhIL-17C (R&D Systems, #9640-IL-025/CF), rhIL-17E (R&D Systems, #8134-IL-025/CF), or rhIL-17F (R&D Systems, #1335-INS-025/CF) for 2 hours. According to the manufacturer's instructions, total RNA was isolated using the Trizol reagent (Ambio, #15596018) and quantified using a Take3 microplate spectrometer (BioTeck, Synergy H1). 1000 ng of RNA was used to synthesize cDNA by reverse transcriptase (Takara, #RR037A). The cDNA was diluted with DNase/RNase-free water 10-fold before performing qPCR. In each qPCR reaction, a mixture in one well of 384-well plates consisted of 2 µl of PCR primer mix (with final concentration of 1 µM and the primer sequences shown in Table 1), 4 µl of SYBR Green Master mix (Applied Biosystems, #A25742), 0.8 µl diluted cDNA, and 1.2 µl DNase/RNase-free water. The following default PCR program was conducted: stage 1 95 ℃ 5 min; stage 2 95 ℃ 15 sec, 60 ℃ 1 min, x 40 cycles; melt curve: 95 ℃ 15 sec, 60 ℃ 1 min, 95 ℃ 15 sec. $^{\Delta\Delta}$Ct method [72] was used to calculate fold change of gene expression. GAPDH was used as loading control and WT-Control group was used for calibration. Fold change relative to Control group of FBXW11 WT of each cell line was calculated as $2^{-\Delta\Delta Ct}$ [($\Delta\Delta Ct$ = sample ($Ct_{target} - Ct_{GAPDH}$) − calibrator ($Ct_{target} - Ct_{GAPDH}$)].

Bioinformatics analysis. Human Protein Atlas database was analyzed to figure out IL-17RA mRNA levels across multiple human cell lines (https://www.proteinatlas.org/, access time 10/27/2022) [73]. Putative phosphodegrons of IL-17RA were predicted by Dr. Pengbo Zhou and eukaryotic linear motif (ELM) resource was explored to further validate this prediction [74]. Multiple sequence alignment of tryptophan-aspartic acid (WD) repeat domain of FBXW family members was conducted with CLUSTAL Omega O(1.2.4)

(https://www.uniprot.org/align) [75]. Proteomics data of glioblastoma multiforme and uterus corpus endometrial carcinoma (UCEC) were downloaded from the Clinical Proteomic Tumor Analysis Consortium (CPTAC) (https://pdc.cancer.gov/pdc/) [76, 77] and UALCAN database (https://ualcan.path.uab.edu/) [78]. Z-values of IL-17RA and FBXW11 protein levels in glioblastoma multiforme, UCEC, and corresponding normal brain and endometrial (with or without enrichment)/myometrial tissues were provided by Dr. Darshan Shimoga Chandrashekar and Dr. Sooryanarayana Varambally at the University of Alabama at Birmingham, which were used to carry out the Pearson's correlation analysis. Phosphorylation abundance of human IL-17RA in UCEC was analyzed using the LinkedOmicsKB platform (https://kb.linkedomics.org/#) [79].

Statistical analysis. All *in vitro* experiments were repeated at least 3 times unless indicated in the figure legends. GraphPad Prism software (Version 9.5.1, 733) was applied to carry out all statistical analysis. A two-way analysis of variance (ANOVA) was conducted to determine the source of variation and its significance when the cells were treated with cycloheximide. Simple linear regression was used to calculate half-life time of proteins when the cells were treated with cycloheximide. One-way ANOVA or unpaired Student's *t* test were applied to determine statistical significance for quantitative data. A two-tailed P value < 0.05 was considered statistically significant.

Acknowledgements

The authors thank Dr. Hua Lu, Dr. Michele Pagano, and Dr. Sachdev Sidhu for gifting plasmids for ubiquitylation assays. We thank Dr. Shelya Zeng and Dr. Jieqiong Wang for guidance on co-immunoprecipitation, ubiquitylation assay, and CRISPR/Cas9-mediated gene knock-out. We thank Dr. Friedemann Weber and Dr. Veit Hornung for kindly sharing A549 FBXW11 WT and A549 FBXW11 KO cell lines. We thank Dr. Hong Liu, Dr. Brain G. Rowan, Dr. Asim B. Abdel-Mageed, and Dr. Yan Dong for insightful discussion of this project. This work was included in Dr. Ben Jin's dissertation in fulfillment of his Ph.D. degree requirements (https://digitallibrary.tulane.edu/islandora/object/tulane%3A139004). Illustration was created with BioRender.com.

This work was primarily funded by the Department of Veteran Affairs (Merit Review Award I01BX004158 to Dr. Zongbing You, Research Physiologist at the Southeast Louisiana Veterans Health Care System, awarded from the Department of Veterans Affairs, Veterans Health Administration, Office of Research and Development, Biomedical Laboratory Research & Development Service) and partially supported by Tulane Cancer Center.

References

1. Monin, L. and S.L. Gaffen, *Interleukin 17 Family Cytokines: Signaling Mechanisms, Biological Activities, and Therapeutic Implications.* Cold Spring Harb Perspect Biol, 2018. **10**(4).
2. Gaffen, S.L., *Structure and signalling in the IL-17 receptor family.* Nat Rev Immunol, 2009. **9**(8): p. 556-67.
3. Huang, J., et al., *Interleukin-17D regulates group 3 innate lymphoid cell function through its receptor CD93.* Immunity, 2021. **54**(4): p. 673-686.e4.
4. Wright, J.F., et al., *The human IL-17F/IL-17A heterodimeric cytokine signals through the IL-17RA/IL-17RC receptor complex.* J Immunol, 2008. **181**(4): p. 2799-805.
5. Su, Y., et al., *Interleukin-17 receptor D constitutes an alternative receptor for interleukin-17A important in psoriasis-like skin inflammation.* Sci Immunol, 2019. **4**(36).
6. Lee, J., et al., *IL-17E, a novel proinflammatory ligand for the IL-17 receptor homolog IL-17Rh1.* J Biol Chem, 2001. **276**(2): p. 1660-4.
7. Wilson, S.C., et al., *Organizing structural principles of the IL-17 ligand-receptor axis.* Nature, 2022. **609**(7927): p. 622-629.
8. Chang, S.H., et al., *Interleukin-17C Promotes Th17 Cell Responses and Autoimmune Disease via Interleukin-17 Receptor E.* Immunity, 2011. **35**(4): p. 611-21.
9. Goepfert, A., et al., *Structural Analysis Reveals that the Cytokine IL-17F Forms a Homodimeric Complex with Receptor IL-17RC to Drive IL-17RA-Independent Signaling.* Immunity, 2020. **52**(3): p. 499-512.e5.
10. Onishi, R.M., et al., *SEF/IL-17R (SEFIR) is not enough: an extended SEFIR domain is required for il-17RA-mediated signal transduction.* J Biol Chem, 2010. **285**(43): p. 32751-32759.
11. Maitra, A., et al., *Distinct functional motifs within the IL-17 receptor regulate signal transduction and target gene expression.* Proc Natl Acad Sci U S A, 2007. **104**(18): p. 7506-11.
12. Pohl, C. and I. Dikic, *Cellular quality control by the ubiquitin-proteasome system and autophagy.* Science, 2019. **366**(6467): p. 818-822.
13. Rape, M., *Ubiquitylation at the crossroads of development and disease.* Nature Reviews Molecular Cell Biology, 2018. **19**(1): p. 59-70.
14. Li, W., et al., *Genome-wide and functional annotation of human E3 ubiquitin ligases identifies MULAN, a mitochondrial E3 that regulates the organelle's dynamics and signaling.* PLoS One, 2008. **3**(1): p. e1487.
15. Rotin, D. and S. Kumar, *Physiological functions of the HECT family of ubiquitin ligases.* Nat Rev Mol Cell Biol, 2009. **10**(6): p. 398-409.
16. Mészáros, B., et al., *Degrons in cancer.* Sci Signal, 2017. **10**(470).
17. Deshaies, R.J. and C.A. Joazeiro, *RING domain E3 ubiquitin ligases.* Annu Rev Biochem, 2009. **78**: p. 399-434.
18. Petroski, M.D. and R.J. Deshaies, *Function and regulation of cullin-RING ubiquitin ligases.* Nat Rev Mol Cell Biol, 2005. **6**(1): p. 9-20.

19. Sarikas, A., T. Hartmann, and Z.Q. Pan, *The cullin protein family.* Genome Biol, 2011. **12**(4): p. 220.
20. Baek, K., et al., *NEDD8 nucleates a multivalent cullin–RING–UBE2D ubiquitin ligation assembly.* Nature, 2020. **578**(7795): p. 461-466.
21. Zhou, Q. and J. Zhang, *K27-linked noncanonic ubiquitination in immune regulation.* J Leukoc Biol, 2022. **111**(1): p. 223-235.
22. Garg, A.V., et al., *The deubiquitinase A20 mediates feedback inhibition of interleukin-17 receptor signaling.* Sci Signal, 2013. **6**(278): p. ra44.
23. Shi, P., et al., *Persistent stimulation with interleukin-17 desensitizes cells through SCFβ-TrCP-mediated degradation of Act1.* Sci Signal, 2011. **4**(197): p. ra73.
24. Qu, F., et al., *TRAF6-dependent Act1 phosphorylation by the IκB kinase-related kinases suppresses interleukin-17-induced NF-κB activation.* Mol Cell Biol, 2012. **32**(19): p. 3925-37.
25. Liu, S., et al., *Hyperinsulinemia enhances interleukin-17-induced inflammation to promote prostate cancer development in obese mice through inhibiting glycogen synthase kinase 3-mediated phosphorylation and degradation of interleukin-17 receptor.* Oncotarget, 2016. **7**(12): p. 13651-66.
26. Winston, J.T., et al., *The SCFbeta-TRCP-ubiquitin ligase complex associates specifically with phosphorylated destruction motifs in IkappaBalpha and beta-catenin and stimulates IkappaBalpha ubiquitination in vitro.* Genes Dev, 1999. **13**(3): p. 270-83.
27. Baek, K., D.C. Scott, and B.A. Schulman, *NEDD8 and ubiquitin ligation by cullin-RING E3 ligases.* Curr Opin Struct Biol, 2021. **67**: p. 101-109.
28. Yada, M., et al., *Phosphorylation-dependent degradation of c-Myc is mediated by the F-box protein Fbw7.* Embo j, 2004. **23**(10): p. 2116-25.
29. Kisselev, A.F., W.A. van der Linden, and H.S. Overkleeft, *Proteasome inhibitors: an expanding army attacking a unique target.* Chem Biol, 2012. **19**(1): p. 99-115.
30. Crawford, L.J., et al., *Comparative selectivity and specificity of the proteasome inhibitors BzLLLCOCHO, PS-341, and MG-132.* Cancer Res, 2006. **66**(12): p. 6379-86.
31. Yim, W.W.-Y. and N. Mizushima, *Lysosome biology in autophagy.* Cell Discovery, 2020. **6**(1): p. 6.
32. Van Roey, K., et al., *Short Linear Motifs: Ubiquitous and Functionally Diverse Protein Interaction Modules Directing Cell Regulation.* Chemical Reviews, 2014. **114**(13): p. 6733-6778.
33. Cardozo, T. and M. Pagano, *The SCF ubiquitin ligase: insights into a molecular machine.* Nature Reviews Molecular Cell Biology, 2004. **5**(9): p. 739-751.
34. Lan, R., et al., *Genome and transcriptome profiling of FBXW family in human prostate cancer.* Am J Clin Exp Urol, 2020. **8**(4): p. 116-128.
35. Zheng, N., et al., *Structure of the Cul1-Rbx1-Skp1-F boxSkp2 SCF ubiquitin ligase complex.* Nature, 2002. **416**(6882): p. 703-9.
36. Draberova, H., et al., *Systematic analysis of the IL-17 receptor signalosome reveals a robust regulatory feedback loop.* Embo j, 2020. **39**(17): p. e104202.
37. Ernst, A., et al., *A strategy for modulation of enzymes in the ubiquitin system.* Science, 2013. **339**(6119): p. 590-5.

38. Gorelik, M., et al., *Inhibition of SCF ubiquitin ligases by engineered ubiquitin variants that target the Cul1 binding site on the Skp1-F-box interface.* Proc Natl Acad Sci U S A, 2016. **113**(13): p. 3527-32.
39. Kainulainen, M., et al., *NSs Virulence Factor of Rift Valley Fever Virus Engages the F-Box Proteins FBXW11 and β-TRCP1 To Degrade the Antiviral Protein Kinase PKR.* J Virol, 2016. **90**(13): p. 6140-7.
40. Frescas, D. and M. Pagano, *Deregulated proteolysis by the F-box proteins SKP2 and beta-TrCP: tipping the scales of cancer.* Nat Rev Cancer, 2008. **8**(6): p. 438-49.
41. Duan, S. and M. Pagano, *Ubiquitin ligases in cancer: Functions and clinical potentials.* Cell Chem Biol, 2021. **28**(7): p. 918-933.
42. Li, X., et al., *IL-17 receptor-based signaling and implications for disease.* Nat Immunol, 2019. **20**(12): p. 1594-1602.
43. Zhao, J., et al., *The role of interleukin-17 in tumor development and progression.* J Exp Med, 2020. **217**(1).
44. Liu, C., et al., *Blocking IL-17A enhances tumor response to anti-PD-1 immunotherapy in microsatellite stable colorectal cancer.* J Immunother Cancer, 2021. **9**(1).
45. McGeachy, M.J., D.J. Cua, and S.L. Gaffen, *The IL-17 Family of Cytokines in Health and Disease.* Immunity, 2019. **50**(4): p. 892-906.
46. Levin, S.D., *IL-17 receptor signaling: ubiquitin gets in on the act.* Sci Signal, 2009. **2**(92): p. pe64.
47. Xu, W. and Y. Huang, *Regulation of Inflammatory Cell Death by Phosphorylation.* Front Immunol, 2022. **13**: p. 851169.
48. Battaglioni, S., et al., *mTOR substrate phosphorylation in growth control.* Cell, 2022. **185**(11): p. 1814-1836.
49. Morrison, D.K., *MAP kinase pathways.* Cold Spring Harb Perspect Biol, 2012. **4**(11).
50. Rong, Z., et al., *Interleukin-17F signaling requires ubiquitination of interleukin-17 receptor via TRAF6.* Cell Signal, 2007. **19**(7): p. 1514-20.
51. Akhoondi, S., et al., *FBXW7/hCDC4 is a general tumor suppressor in human cancer.* Cancer Res, 2007. **67**(19): p. 9006-12.
52. Nateri, A.S., et al., *The ubiquitin ligase SCFFbw7 antagonizes apoptotic JNK signaling.* Science, 2004. **303**(5662): p. 1374-8.
53. Cheng, Y. and G. Li, *Role of the ubiquitin ligase Fbw7 in cancer progression.* Cancer and Metastasis Reviews, 2012. **31**(1): p. 75-87.
54. Lau, A.W., H. Fukushima, and W. Wei, *The Fbw7 and betaTRCP E3 ubiquitin ligases and their roles in tumorigenesis.* Front Biosci (Landmark Ed), 2012. **17**(6): p. 2197-212.
55. Knizkova, D., et al., *CMTM4 is a subunit of the IL-17 receptor and mediates autoimmune pathology.* Nat Immunol, 2022. **23**(11): p. 1644-1652.
56. Kim, T.Y., et al., *Substrate trapping proteomics reveals targets of the βTrCP2/FBXW11 ubiquitin ligase.* Mol Cell Biol, 2015. **35**(1): p. 167-81.
57. Swatek, K.N. and D. Komander, *Ubiquitin modifications.* Cell Res, 2016. **26**(4): p. 399-422.
58. Yau, R. and M. Rape, *The increasing complexity of the ubiquitin code.* Nat Cell Biol, 2016. **18**(6): p. 579-86.

59. Tracz, M. and W. Bialek, *Beyond K48 and K63: non-canonical protein ubiquitination.* Cell Mol Biol Lett, 2021. **26**(1): p. 1.
60. Kathania, M., et al., *Itch inhibits IL-17-mediated colon inflammation and tumorigenesis by ROR-γt ubiquitination.* Nat Immunol, 2016. **17**(8): p. 997-1004.
61. Nakasone, M.A., et al., *Mixed-linkage ubiquitin chains send mixed messages.* Structure, 2013. **21**(5): p. 727-40.
62. Gao, D., et al., *mTOR drives its own activation via SCF(βTrCP)-dependent degradation of the mTOR inhibitor DEPTOR.* Mol Cell, 2011. **44**(2): p. 290-303.
63. Hunter, T., *The age of crosstalk: phosphorylation, ubiquitination, and beyond.* Mol Cell, 2007. **28**(5): p. 730-8.
64. Li, X. and Y. Song, *Proteolysis-targeting chimera (PROTAC) for targeted protein degradation and cancer therapy.* J Hematol Oncol, 2020. **13**(1): p. 50.
65. Prescott, J.A., J.P. Mitchell, and S.J. Cook, *Inhibitory feedback control of NF-κB signalling in health and disease.* Biochem J, 2021. **478**(13): p. 2619-2664.
66. Chen, Y., et al., *Ubiquitin ligase TRIM71 suppresses ovarian tumorigenesis by degrading mutant p53.* Cell Death & Disease, 2019. **10**(10): p. 737.
67. Qian, Y., et al., *The adaptor Act1 is required for interleukin 17-dependent signaling associated with autoimmune and inflammatory disease.* Nat Immunol, 2007. **8**(3): p. 247-56.
68. You, Z., et al., *Differential expression of IL-17RC isoforms in androgen-dependent and androgen-independent prostate cancers.* Neoplasia, 2007. **9**(6): p. 464-70.
69. Ran, F.A., et al., *Genome engineering using the CRISPR-Cas9 system.* Nat Protoc, 2013. **8**(11): p. 2281-2308.
70. Shalem, O., et al., *Genome-scale CRISPR-Cas9 knockout screening in human cells.* Science, 2014. **343**(6166): p. 84-87.
71. van Kley, H. and S.M. Hale, *Assay for protein by dye binding.* Anal Biochem, 1977. **81**(2): p. 485-7.
72. Livak, K.J. and T.D. Schmittgen, *Analysis of relative gene expression data using real-time quantitative PCR and the 2(-Delta Delta C(T)) Method.* Methods, 2001. **25**(4): p. 402-8.
73. Karlsson, M., et al., *A single-cell type transcriptomics map of human tissues.* Sci Adv, 2021. **7**(31).
74. Kumar, M., et al., *The Eukaryotic Linear Motif resource: 2022 release.* Nucleic Acids Res, 2022. **50**(D1): p. D497-d508.
75. Sievers, F. and D.G. Higgins, *Clustal Omega for making accurate alignments of many protein sequences.* Protein Sci, 2018. **27**(1): p. 135-145.
76. Dou, Y., et al., *Proteogenomic Characterization of Endometrial Carcinoma.* Cell, 2020. **180**(4): p. 729-748.e26.
77. Wang, L.B., et al., *Proteogenomic and metabolomic characterization of human glioblastoma.* Cancer Cell, 2021. **39**(4): p. 509-528.e20.
78. Chandrashekar, D.S., et al., *UALCAN: An update to the integrated cancer data analysis platform.* Neoplasia, 2022. **25**: p. 18-27.
79. Zhang, S.R.S.Y.L.Y.D.Z.S.X.Y.W.J.J.T.L.B. *LinkedOmicsKB: A web portal to explore pan-cancer molecular and phenotype associations* in *AACR*. 2023. Orlando: Cancer Res.

967 # Figure and Corresponding Legends

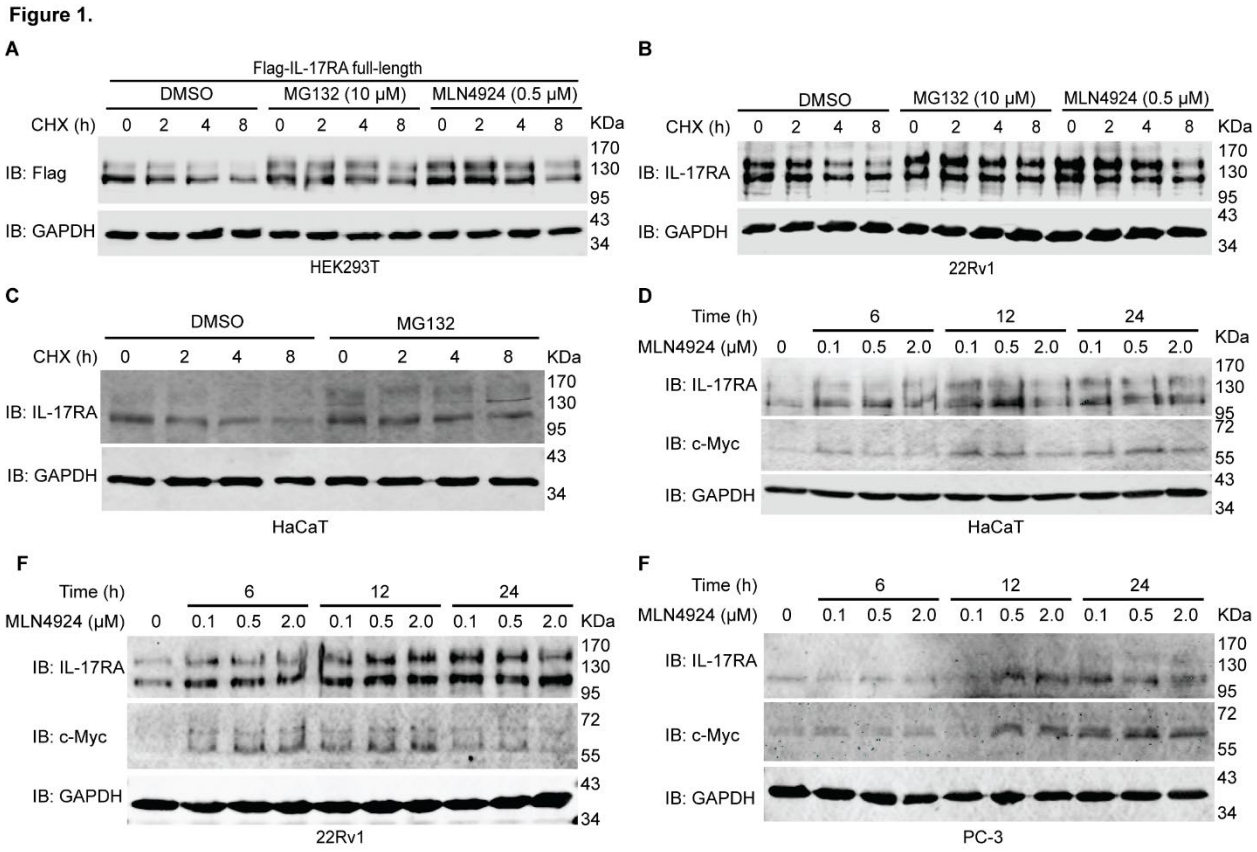

968

969 **Figure 1. Exogenous and endogenous IL-17RA are degraded through ubiquitin-**
970 **proteasome system, particularly Cullin-Ring-E3 Ligase complex.**
971 **(A)** Western Blot analysis of expression levels of exogenous Flag-IL-17RA. 5 μg full-
972 length Flag-IL-17RA plasmids were transiently transfected into HEK293T cells in a 10-cm
973 dish. 18 hours (h) post transfection, cells were evenly split into 6-well plates. 42 h post
974 transfection, the cells were treated with 20 μM MG132 or 0.5 μM MLN4924 for 8 h and
975 50 μg/ml CHX for indicated hours. Of note, in the group with CHX treatment for 8 h,
976 MG132 or MLN4924 was added to all treatment groups simultaneously. Treatment of
977 each subgroup was terminated at the same time, therefore CHX was added to another
978 two subgroups 2 and 4 h before collecting cells. Overall, treatment time of MG132 and
979 MLN4924 was 8 h and treatment time of CHX was 0, 2, 4, and 8 h, respectively. DMSO
980 was used as control treatment. **(B)** Western blot analysis of endogenous IL-17RA in
981 22Rv1 cells after treatment with 20 μM MG132, 0.5 μM MLN4924 for 8h and 50 μg/ml
982 CHX for indicated hours. DMSO was used as control treatment. **(C)** Western blot analysis
983 of endogenous IL-17RA in HaCaT cell line after treatment with 10 μM of MG132 for 8 h
984 and 50 μg/ml of CHX for indicated time. DMSO was used as control treatment. **(D-F)**
985 Neddylation inhibitor MLN4924 at 0.1 μM, 0.5 μM, and 2.0 μM was used to treat HaCaT
986 **(D)**, 22Rv1 **(E)** and PC-3 **(F)** cell lines for 6, 12 and 24 h. DMSO was used as control
987 treatment. Each experiment was repeated at least 3 times.
988

Figure 1-figure supplement 1

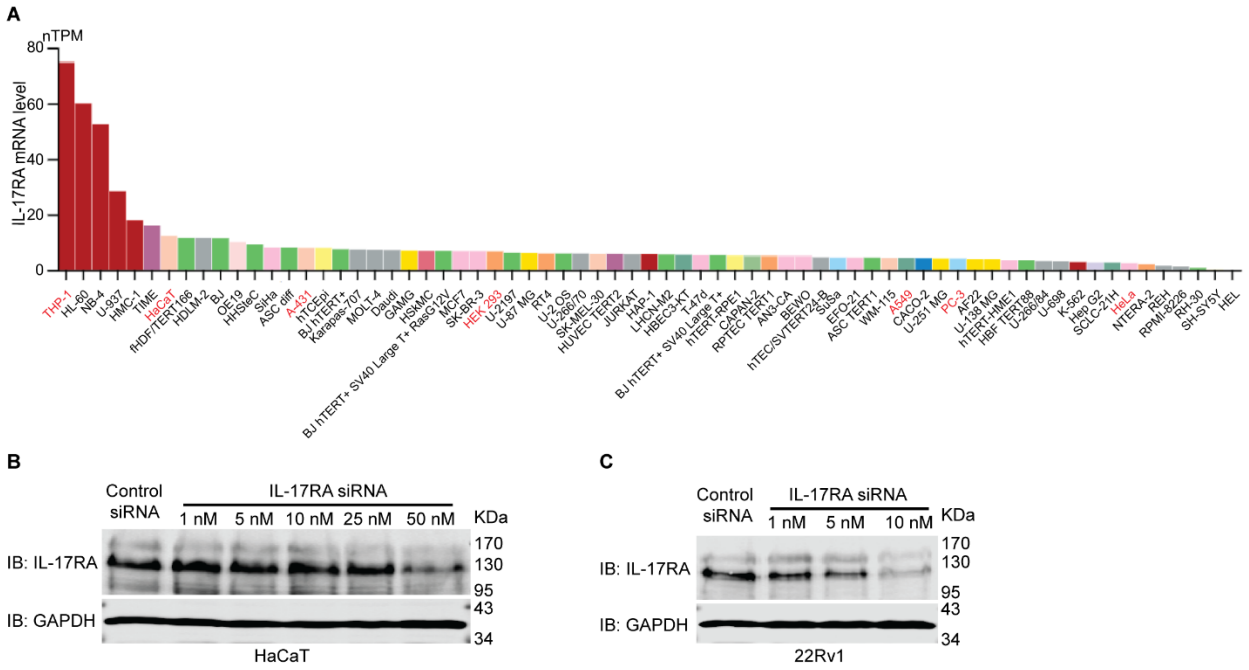

Figure 1-figure supplement 1. Expression level of endogenous IL-17RA mRNAs across multiple cell lines and validation of the specificity of anti-IL-17RA antibody. **(A)** Human Protein Atlas database (https://www.proteinatlas.org/; access date 10/27/2022) was explored to figure out mRNA levels of IL-17RA across multiple human cell lines. **(B & C)** To validate the specificity of anti-IL-17RA antibody (G9 clone, Santa Cruz Biotechnology), HaCaT cells in 10-cm dishes **(B)** and 22Rv1 cells in 6-cm dishes **(C)** were transiently transfected with various amounts of IL-17RA siRNA or control siRNA for 48 h. Protein levels of endogenous IL-17RA were analyzed using Western blot.

Figure 1-figure supplement 2

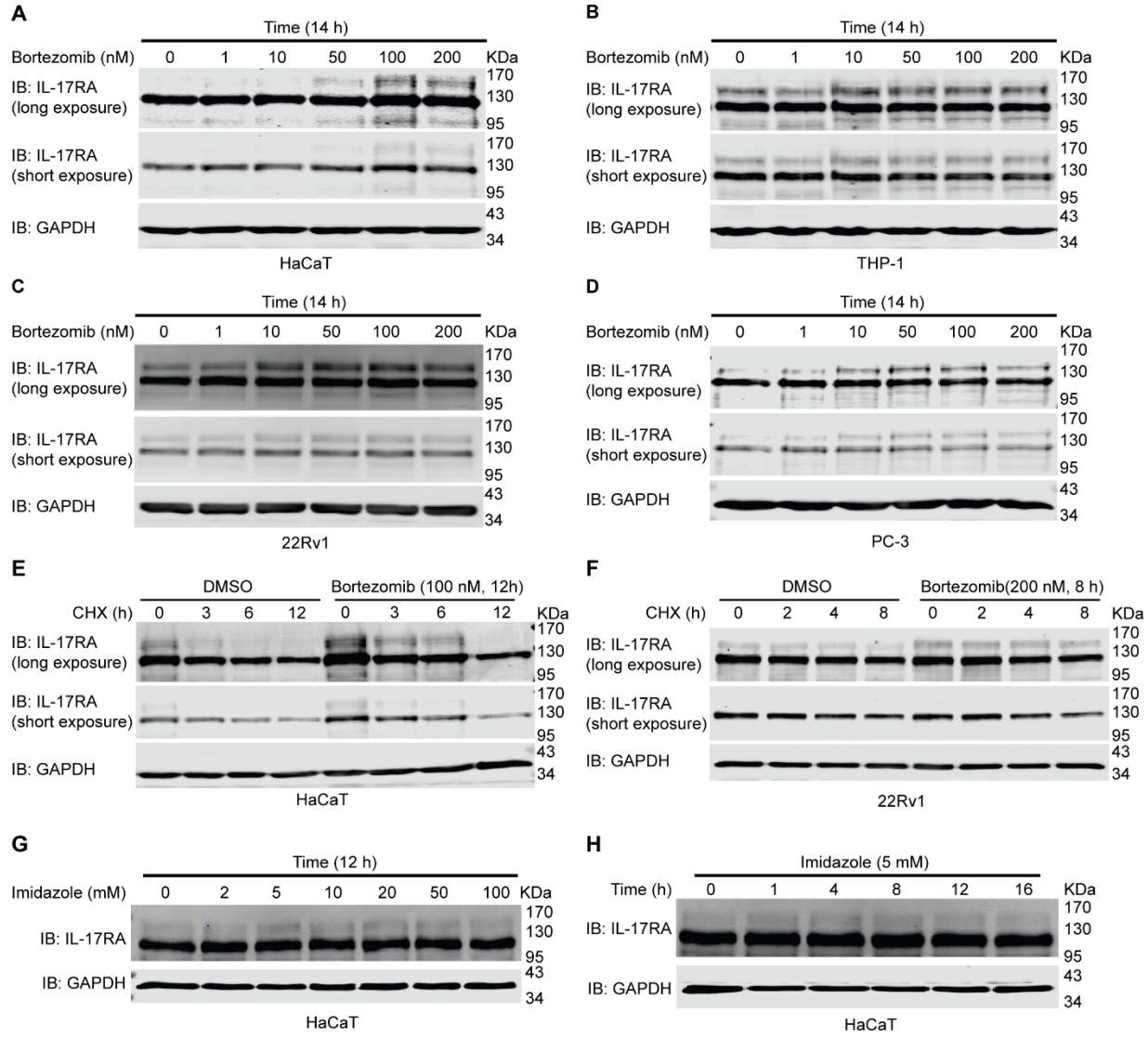

Figure 1-figure supplement 2. Proteasome inhibitor bortezomib slightly accumulates endogenous IL-17RA but lysosome inhibitor imidazole has no obvious effect on IL-17RA protein levels.

(A-D) Western blot analysis of endogenous IL-17RA in HaCaT **(A)**, THP-1 **(B)**, 22Rv1 **(C)**, and PC-3 **(D)** cell lines treated with 1 nM, 10 nM, 50 nM, 100 nM, and 200 nM bortezomib for 14 h. DMSO was used as control treatment. **(E)** Western blot analysis of endogenous IL-17RA in HaCaT cell line treated with 100 nM bortezomib for 12 h and 50 μg/ml CHX for indicated time. DMSO was used as control treatment. **(F)** Western blot analysis of endogenous IL-17RA in 22Rv1 cell line treated with 200 nM bortezomib for 8 h and 50 μg/ml CHX for indicated time. DMSO was used as control treatment. **(G)** Western blot analysis of endogenous IL-17RA in HaCaT cell line treated with 2 mM, 5 mM, 10 mM, 20 mM, 50 mM, and 100 mM imidazole for 12 h. DMSO was used as control treatment. **(H)** Western blot analysis of endogenous IL-17RA in HaCaT cell line treated with 5 mM imidazole for indicated time. DMSO was used as control treatment. Treatment of bortezomib was repeated 3 times while treatment of imidazole was repeated 2 times.

Figure 2.

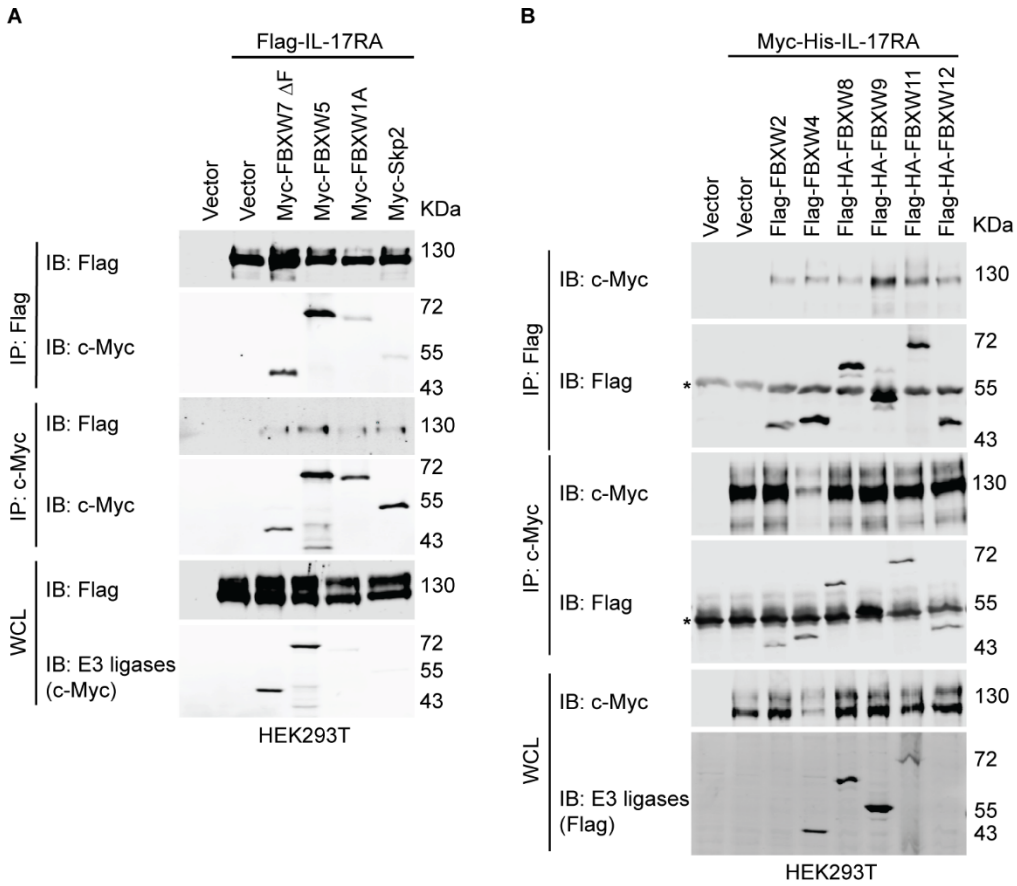

Figure 2. Several FBXW E3 ligases bind to IL-17RA.
(A) Binding of IL-17RA with E3 ligases. HEK293T cells were seeded at a density of 1 x 10^6 into 6-cm dishes. 20 h post-seeding, 1.5 µg full-length Flag-IL-17RA, 1.5 µg Myc-FBXW7 ΔF, 1.5 µg Myc-FBXW5, 1.5 µg Myc-FBXW1A and 1.5 µg Myc-Skp2 plasmids were transiently transfected using jetPRIME transfection reagent as indicated. An empty vector was used to compensate for the total amount of plasmids. 48 h post transfection, proteins were extracted using IP lysis buffer. The reciprocal co-IP assays were carried out using 1 µg anti-Flag M2 or 1 µg anti-c-Myc antibodies. Experiments were repeated 4 times independently. **(B)** Binding of IL-17RA with E3 ligases. HEK293T cells were seeded at a density of 1 x 10^6 into 6-cm dishes. 2 µg full-length Myc-His-IL-17RA, 2 µg Flag-FBXW2, 2 µg Flag-FBXW4, 1.5 µg Flag-HA-FBXW8, 1 µg Flag-HA-FBXW9, 2 µg Flag-HA-FBXW11, and 2 µg Flag-FBXW12 plasmids were transiently transfected using jetPRIME transfection reagent as indicated. An empty vector was used to compensate for the total amount of plasmids. 48 h post transfection, proteins were extracted using IP lysis buffer. The reciprocal co-IP assays were carried out using 1 µg anti-Flag M2 or 1 µg anti-c-Myc antibodies. Experiments were repeated 3 times independently. Asterisks indicate IgG heavy chain of antibodies used in co-IP. Experiments were repeated 4 times independently.

Figure 2-figure supplement 1.

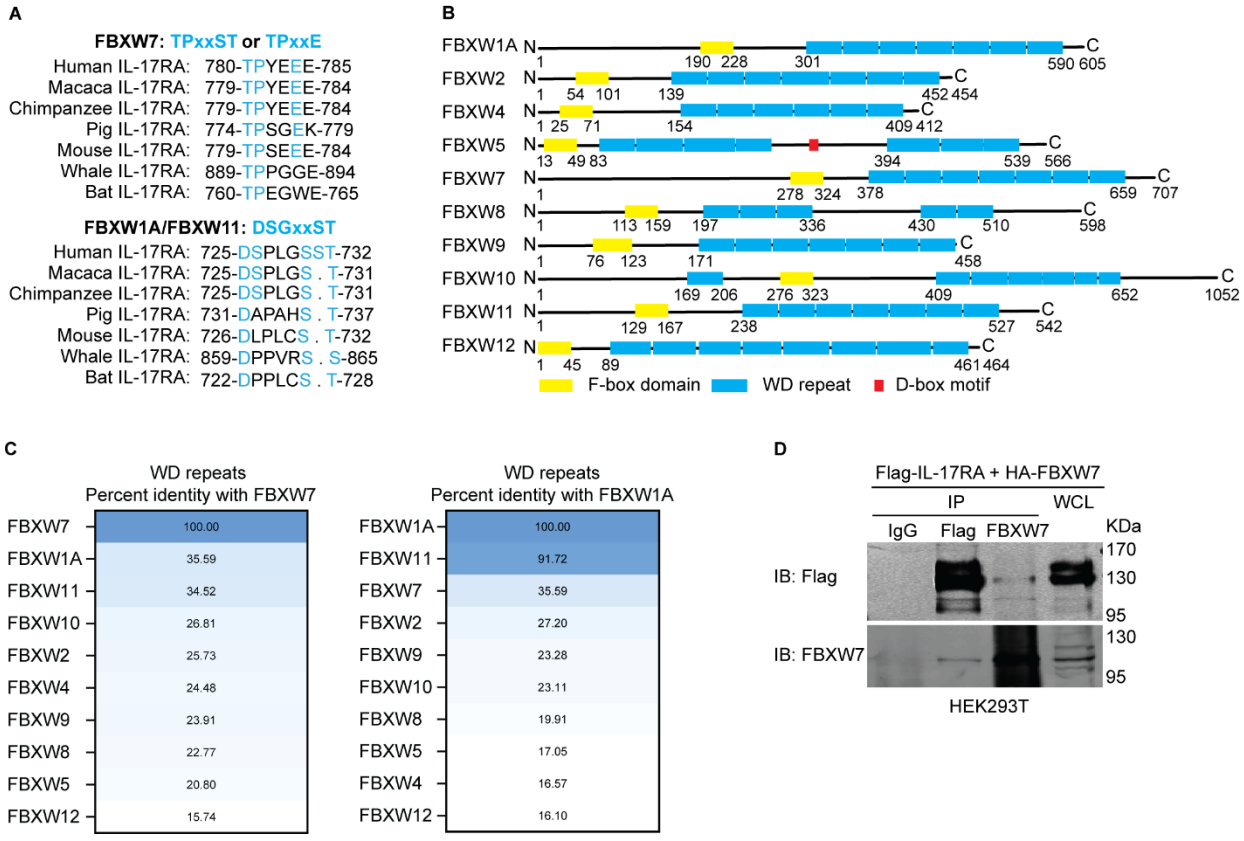

Figure 2-figure supplement 1. F-box and WD repeat domain containing 7 (FBXW7) and FBXW1A/11 are E3 ligase candidates recognizing IL-17RA phosphodegron. **(A)** Phosphodegron TPxxE recognized by FBXW7 matches amino acid 780-785 of human IL-17RA. Phosphodegron DSGxxST recognized by FBXW1A/11 matches amino acid 725-732 of human IL-17RA. The phosphodegrons are conserved across different species. **(B)** Diagram showing conserved domains, F-box domain and WD repeat domain, of FBXW family members. FBXW5 has a special D-box domain. **(C)** Percent identity of tryptophan-aspartic acid (WD) repeat domains of FBXW family members was computed with Clustal Omega algorithm [75]. The plot was made using Prism GraphPad. **(D)** Binding of IL-17RA with FBXW7. HEK293T cells were seeded into 6-cm dishes at the density of 1 x 10^6. 1.5 µg full-length Flag-IL-17RA and 1.5 µg full-length HA-FBXW7 plasmids were transiently transfected using jetPRIME transfection reagent. An empty vector was used to compensate for the total amount of plasmids. 48 h post transfection, proteins were extracted using IP lysis buffer. The co-IP assays were carried out using 2 µg normal IgG (Cell signaling technology, #2729), 2 µg anti-Flag M2 or 12 µg anti-FBXW7. Experiments were repeated 4 times independently.

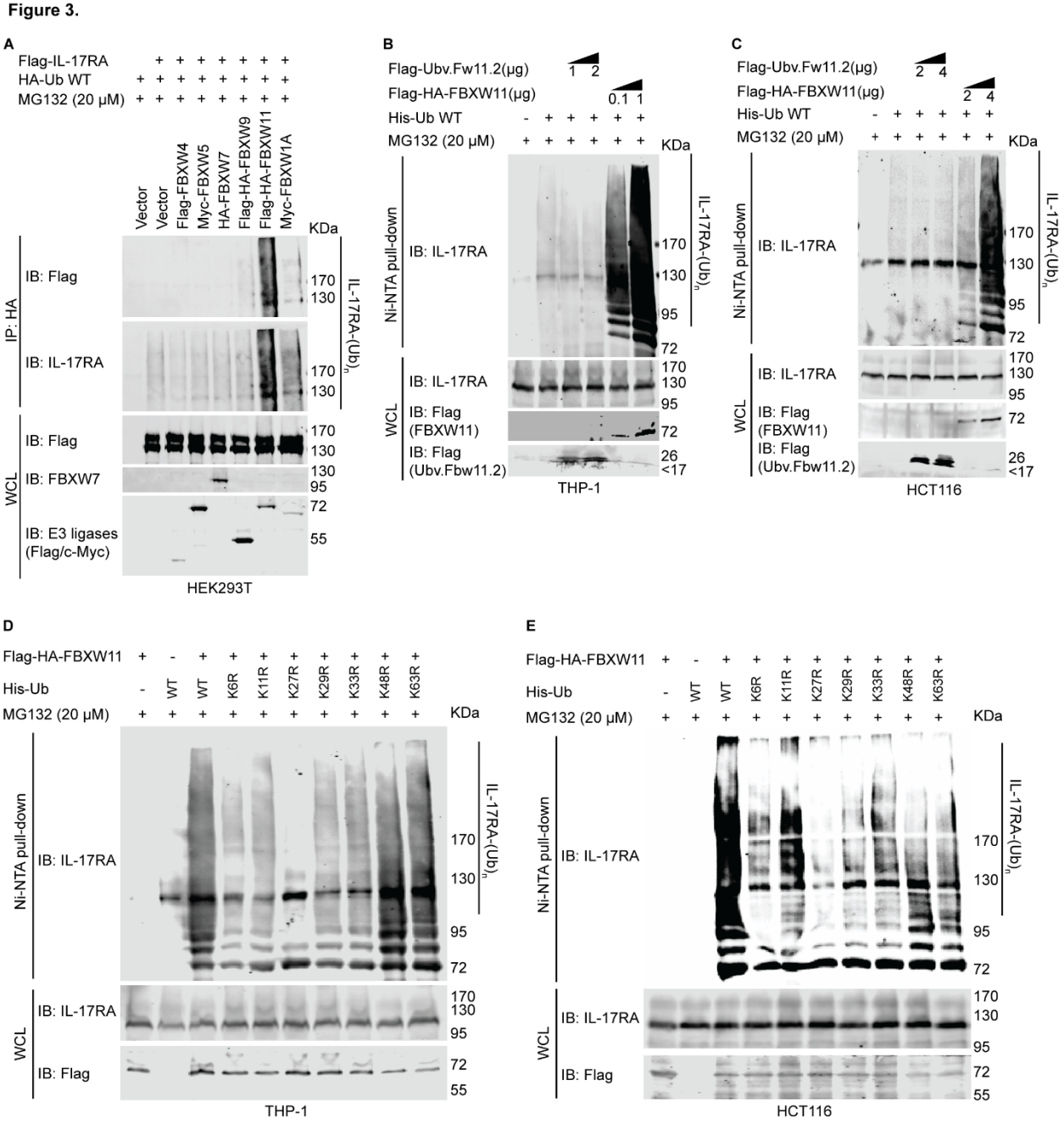

Figure 3. FBXW11 ubiquitylates IL-17RA mainly via K27-linked polyubiquitin chain in a dose-dependent way.

(A) HEK293T cells were seeded into 10-cm dishes at a density of 4 x 10^6. 3 μg full-length Flag-IL-17RA, 2 μg HA-ubiquitin WT, 3 μg Flag-FBXW4, 3 μg Myc-FBXW5, 4 μg HA-FBXW7, 2 μg Flag-HA-FBXW9, 3 μg Flag-HA-FBXW11, and 3 μg Myc-FBXW1A plasmids were transiently transfected using jetPRIME transfection reagent as indicated. An empty vector was used to compensate for the total amount of plasmids. 42 h post transfection, transfected cells were treated with 10 μM MG132 for 6 h. Experiments were repeated 4 times independently. **(B)** THP-1 cells were seeded into 10-cm dishes at a density of 1.5 x 10^6. 24 h post seeding, 1 or 2 μg Flag-Ubv.Fw.11.2, 0.1 or 1 μg Flag-

HA-FBXW11, and 2.5 µg His-ubiquitin WT plasmids were transfected using JetPrime transfection reagent. An empty vector was used to compensate for the total amount of plasmids. 42 h post transfection, 20 µM MG132 was added to treat the cells for 6 h. **(C)** HCT116 cells were seeded into 10-cm dishes at the density of 2 x 10^6. 24 h post seeding, 2 or 4 µg Flag-Ubv.Fw.11.2, 2 or 4 µg Flag-HA-FBXW11, and 2.5 µg His-ubiquitin WT plasmids were transfected using JetPrime transfection reagent. An empty vector was used to compensate for the total amount of plasmids. 42 h post transfection, 20 µM MG132 was added to treat the cells for 6 h. Experiments were repeated 4 times independently. **(D)** THP-1 cells were seeded into 10-cm dishes at a density of 1.5 x 10^6. 24 h post-seeding, 1 µg Flag-HA-FBXW11, and 2.5 µg WT or single lysine mutated His-ubiquitin plasmids were transfected using JetPrime transfection reagent. Empty vector was used to compensate for the total amount of plasmids in transfection. 42 h post-transfection, 20 µM MG132 was added to treat the cells for 6 h. Experiments were repeated 4 times independently. **(E)** HCT116 cells were seeded into 10-cm dishes at a density of 3 x 10^6. 24 h post-seeding, 2 or 4 µg Flag-HA-FBXW11, and 2.5 µg WT or single lysine mutated His-ubiquitin plasmids were transfected using JetPrime transfection reagent. Empty vector was used to compensate for the total amount of plasmids in transfection. 42 h post-transfection, 20 µM MG132 was added to treat the cells for 6 h. Experiments were repeated 3 times independently.

Figure 3-figure supplement 1.

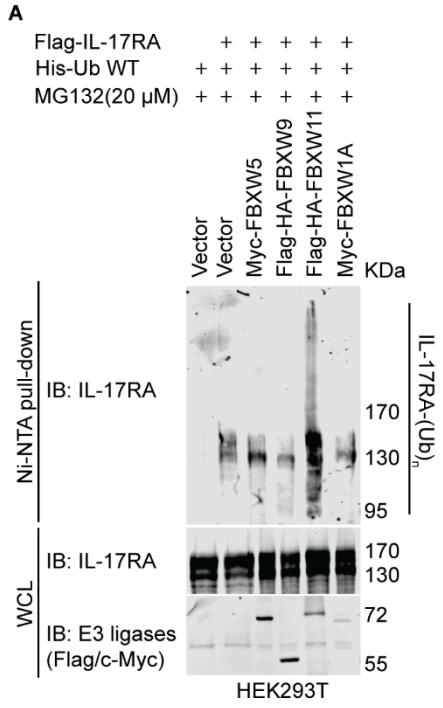

Figure 3-figure supplement 1. FBXW11 has the highest ubiquitylation activity towards IL-17RA.

(A) 21 h before transfection, HEK293T cells were seeded into 10-cm dishes at a density of 4.5 x 10^6. 1.5 μg full-length Flag-IL17RA, 3 μg His-ubiquitin WT, 2 μg Myc-FBXW5, 1.5 μg Flag-HA-FBXW9, 3.5 μg Flag-HA-FBXW11, 3.5 μg Myc-FBXW1A, and various amounts of empty vector (to compensate for the total amount of plasmids) were transiently transfected using jetPRIME transfection reagent as indicated; 40 h post transfection, 20 μM MG132 was added to treat cells for 8 h.

Figure 4.

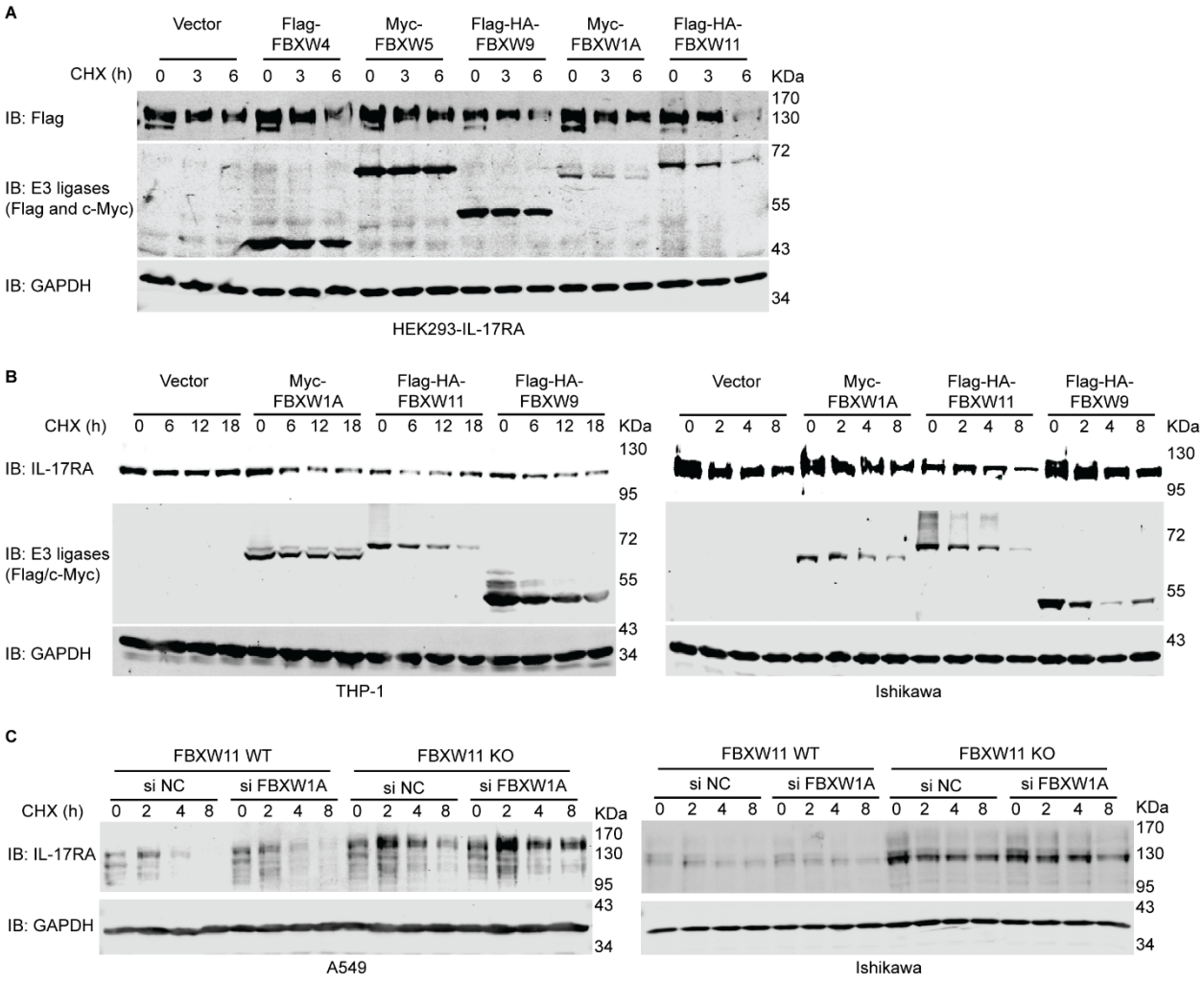

Figure 4. FBXW11 down-regulates the protein level of IL-17RA.
(A) CHX assays were conducted to investigate the effects of FBXW1A, FBXW9, and FBXW11 overexpression on HEK293-IL-17RA stable cell line. 24 h before transfection, 1.2 x 10^6 HEK293-IL-17RA cells were seeded into 6-cm dishes. 2 µg Flag-FBXW4, 1.5 µg Myc-FBXW5, 1.5 µg Flag-HA-FBXW9, 3 µg Myc-FBXW1A, or 3 µg Flag-HA-FBXW11 plasmids were transiently transfected using jetPRIME transfection reagent. Empty vector was used as transfection control and to compensate for the total amount of plasmids for each transfection. 6 h post-transfection, the cells in each 6-cm dish were evenly split into 3 wells of a 6-well plate. 24 h post-transfection, the cells were treated with 100 µg/ml CHX for 0, 3, and 6 h, respectively. DMSO was used as control treatment. **(B)** CHX assays were conducted to investigate the effects of FBXW1A, FBXW9, and FBXW11 on endogenous IL-17RA protein levels in THP-1 (left panel) and Ishikawa (right panel) cell lines. For THP-1 cells, 1.0 x 10^6 cells were seeded into 6-cm dishes 24 h before transfection, and 4 µg Myc-FBXW1A, 1.5 µg Flag-HA-FBXW9, or 5 µg Flag-HA-FBXW11 were transiently transfected using jetPRIME transfection reagent. Empty vector was used as a transfection control and to compensate for the total amount of plasmids in each

transfection. 24 h post-transfection, the cells were treated with 100 μg/ml CHX for 0, 6, 12, and 18 h, respectively, with DMSO used as control treatment. For Ishikawa cells, 3.5 x 10^6 cells were seeded into 10-cm dishes 24 h before transfection, and 9 μg Myc-FBXW1A, 3 μg Flag-HA-FBXW9, or 10 μg Flag-HA-FBXW11 plasmids were transiently transfected using jetPRIME transfection reagent. Empty vector was used as a transfection control and to compensate for the total amount of plasmids in each transfection. 12 h post-transfection, the cells in each 10-cm dish were evenly split into four 6-cm dishes. 36 h post-transfection, the cells were treated with 100 μg/ml CHX for 0, 2, 4, and 8 h, respectively, with DMSO used as control treatment. The experiments were independently repeated 3 times. **(C)** CHX assays were conducted to investigate the effects of FBXW11 knock-out combined with/without FBXW1A knock-down on A549 (left panel) and Ishikawa (right panel) cell lines. For both cell lines, 2.0 x 10^6 FBXW11 WT or 2.5 x 10^6 FBXW11 KO cells were seeded into 10-cm dishes 24 h before transfection, and 20 nM FBXW1A siRNAs were transiently transfected using jetPRIME transfection reagent. Negative control siRNAs were used as control. 24 h post-transfection, the cells in each 10-cm dish were split evenly into four 6-cm dishes. 48 h post-transfection, cells were treated with 50 μg/ml CHX for 0, 2, 4, and 8 h, respectively, with DMSO used as control treatment. The experiments were independently repeated 3 times.

Figure 5.

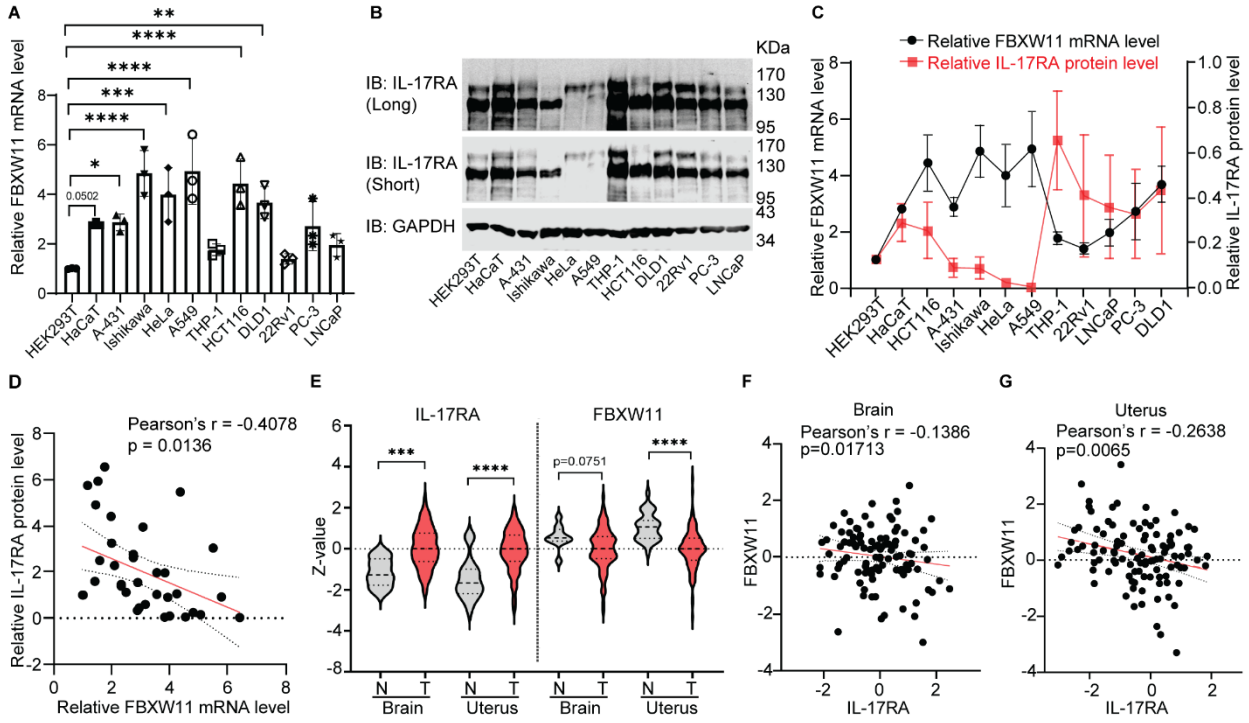

Figure 5. FBXW11 and IL-17RA are inversely correlated.

(A) Total RNA was isolated from 12 cell lines, including HEK293T, HaCaT, A-431, Ishikawa, HeLa, A549, THP-1, HCT116, DLD1, 22RV1, PC-3, and LNCaP. Real-time qPCR analysis was conducted to measure FBXW11 mRNA levels. HEK293T cell line was used as calibration control and Student's *t* test was used to determine statistical significance when compared to HEK293T. ** P< 0.01, *** P< 0.001, and **** P< 0.0001. Data were collected from 3 independent biological replicates. **(B)** Western blot analysis was used to determine IL-17RA protein levels across 12 cell lines, including HEK293T, HaCaT, A-431, Ishikawa, HeLa, A549, THP-1, HCT116, DLD1, 22RV1, PC-3, and LNCaP. "Long" indicates long exposure and "Short" indicates short exposure. Signal intensities of IL-17RA and Glyceraldehyde-3-Phosphate Dehydrogenase (GAPDH) in each cell line were determined using Image Studio (Lite Ver 5.2, Li-Cor) software. The ratio of IL-17RA/GAPDH was then calculated to compare relative protein levels. HEK293T cell line was used as calibration control. Data were collected from 3 independent replicates. **(C)** The quantification results shown in **(A)** and **(B)** were plotted to illustrate the trajectory of relative FBXW11 mRNA levels and IL-17RA protein levels across the 12 human cell lines. Error bar represents mean ± standard deviation (S.D.). **(D)** Pearson's correlation analysis was conducted using the data of relative FBXW11 mRNA levels and relative IL-17RA protein levels. **(E)** Proteomic data obtained from CPTAC database demonstrated IL-17RA and FBXW11 protein levels among glioblastoma multiform (brain tumors), uterus corpus endometrial cancer (UCEC, uterine tumors) and corresponding normal control tissues. Z-value indicates standard deviations from the median across samples for the given cancer type. The Student's *t* test was used to determine statistical significance between normal

control tissues and tumors. *** P < 0.001 and **** P <0.0001. **(F)** Pearson's correlation analysis was conducted using the proteomic data on FBXW11 and IL-17RA protein levels of glioblastoma multiform and normal control tissues. **(G)** Pearson's correlation analysis was conducted using the proteomic data on FBXW11 and IL-17RA protein levels of UCEC and normal control tissues. Control tissues of glioblastoma were from the frontal cortex. Control tissues of uterine tumors were from endometrium (with or without enrichment) and myometrium.

Figure 5-figure supplement 1.

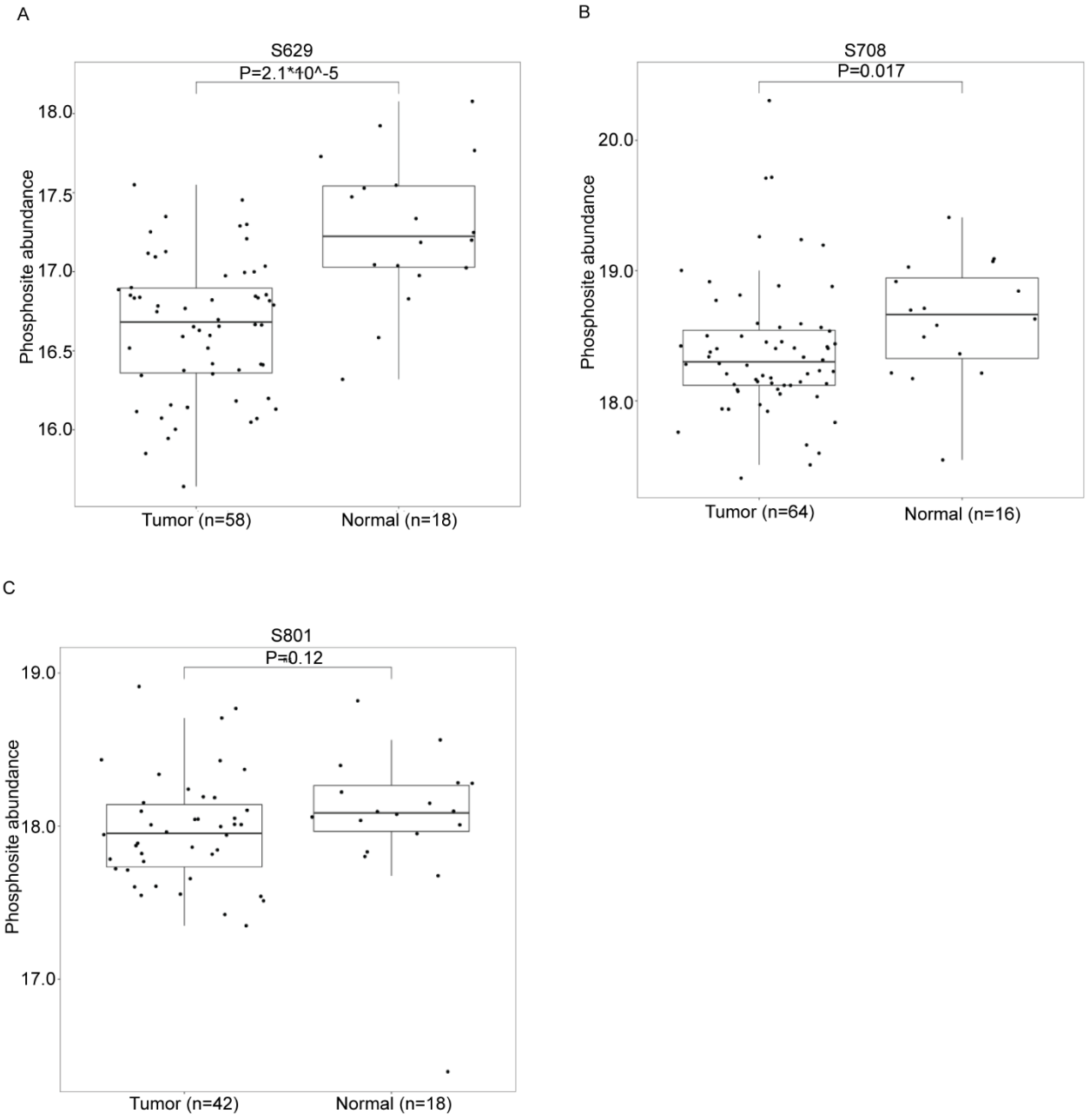

Figure 5-figure supplement 1. Phosphosite abundance of IL-17RA in UCEC and Normal tissue.

(A) Phosphosite abundance data obtained from the LinkedOmicsKB platform showed that phosphorylation of S629 in UCEC was significantly lower than normal control. **(B)** Phosphosite abundance data obtained from the LinkedOmicsKB platform showed that phosphorylation of S708 in UCEC was significantly lower than normal control. **(C)** Phosphosite abundance data obtained from the LinkedOmicsKB platform showed that phosphorylation of S801 in UCEC was slightly lower than normal control without statistical significance.

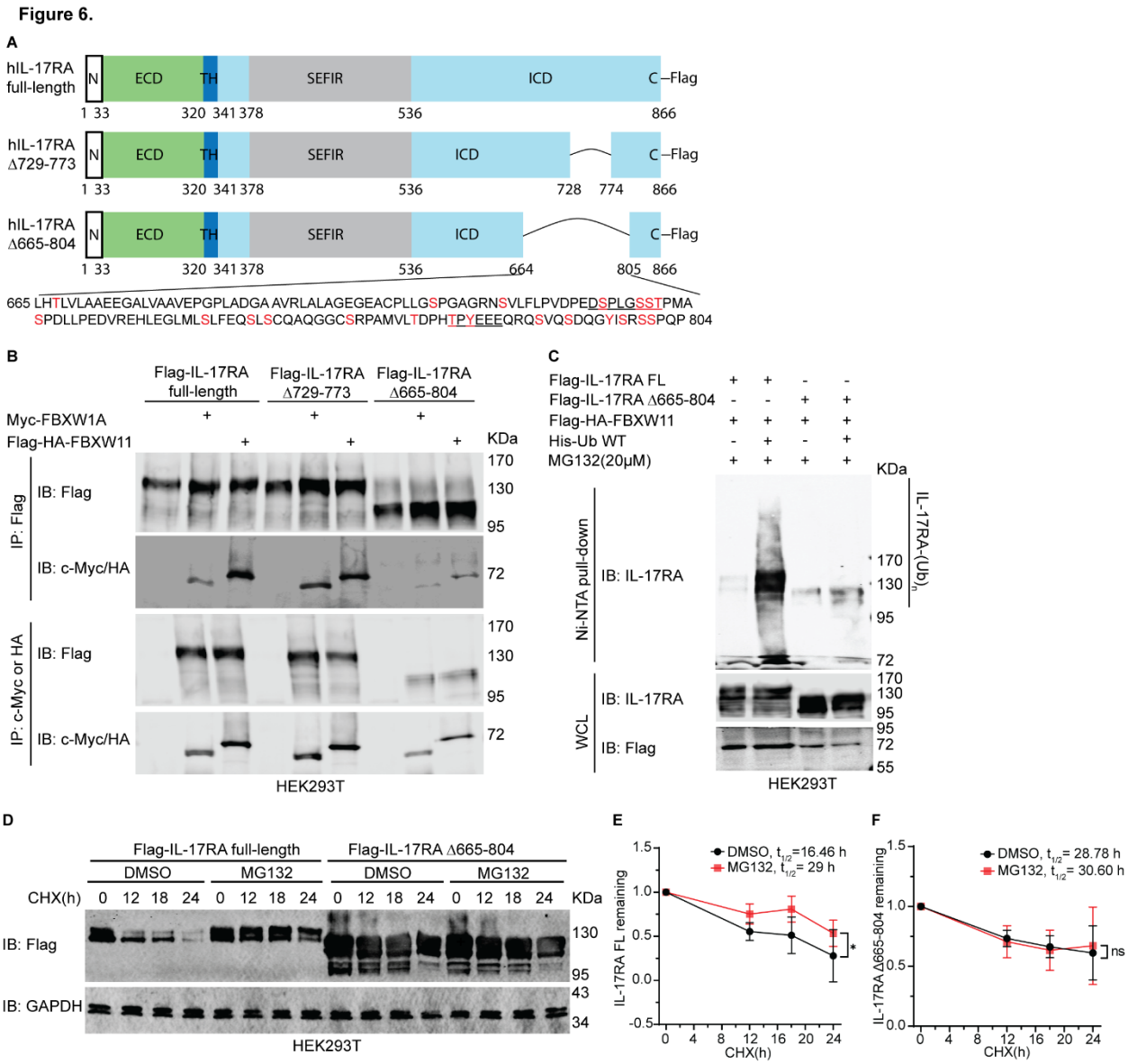

Figure 6. 665-804 domain of IL-17RA is required for ubiquitylation and protein stability of IL-17RA.

(A) Schematic diagram of full-length IL-17RA (Flag-IL-17RA FL) and truncated mutants (Flag-IL-17RA Δ729-773 and Flag-IL-17RA Δ665-804) used in this study. **(B)** Binding of full-length IL-17RA and truncated mutants with FBXW1A and FBXW11. HEK293T cells were seeded into 10-cm dishes at a density of 2.0 x 10^6. 20 h post-seeding, 1.5 μg Flag-IL-17RA FL, 1.5 μg Flag-IL-17RA Δ729-773, 1 μg Flag-IL-17RA Δ665-804, 1.5 μg Myc-FBXW1A, and 1.5 μg Flag-HA-Fbxw11 were transiently transfected using jetPRIME transfection reagent as indicated. Empty vector was used to compensate for the total amount of plasmids in transfection. 48 h post transfection, the whole cell lysates were extracted for subsequent co-IP and Western blot analyses. **(C)** Ubiquitylation of Flag-IL-17RA Δ665-804 by FBXW11 was less than Flag-IL-17RA FL. HEK293T cells were seeded into 10-cm dishes at a density of 4.5 x 10^6. 24 h post-seeding, 1 μg Flag-IL-17RA full-

length, 0.75 μg Flag-IL-17RA Δ665-804, 3.5 μg Flag-HA-FBXW11, 2.5 μg His-ubiquitin WT plasmids were transfected using jetPRIME transfection reagent as indicated. 40 h post-transfection, the cells were treated with 20 μM MG132 for 8 h. Precipitates pulled-down by Ni-NTA resins and corresponding whole cell lysate (WCL) were subject to Western blot analysis. **(D)** Western Blot analysis of protein stability of Flag-IL-17RA FL and Flag-IL-17RA Δ665-804. 1.5 μg Flag-IL-17RA FL or 1.5 μg Flag-IL-17RA Δ665-804 plasmids were transiently transfected into 1.5 x 10^6 HEK293T cells in a 6-cm dish. 24 h post-transfection, the cells were treated with 10 μM MG132 for 24 h and 50 μg/ml CHX for indicated time. DMSO was applied as control treatment. Experiments were repeated 4 times independently. **(E)** Quantification of ratio of exogenous Flag-IL-17RA FL/GAPDH after treatment with MG132 and CHX. The $t_{1/2}$ means half-life of IL-17RA FL. Statistical significance was conducted using a two-way ANOVA with Šídák's multiple comparison test. Error bar represents mean ± standard deviation (S.D.). * $P < 0.05$. **(F)** Quantification of ratio of exogenous Flag-IL-17RA Δ665-804 to GAPDH after treatment with MG132 and CHX. The $t_{1/2}$ means half-life of IL-17RA Δ665-804. Statistical significance was computed using a two-way ANOVA with Šídák's multiple comparison test. Error bar represents mean ± standard deviation (S.D.). The “ns” means no statistical significance. Experiments were repeated 3 times independently.

Figure 7.

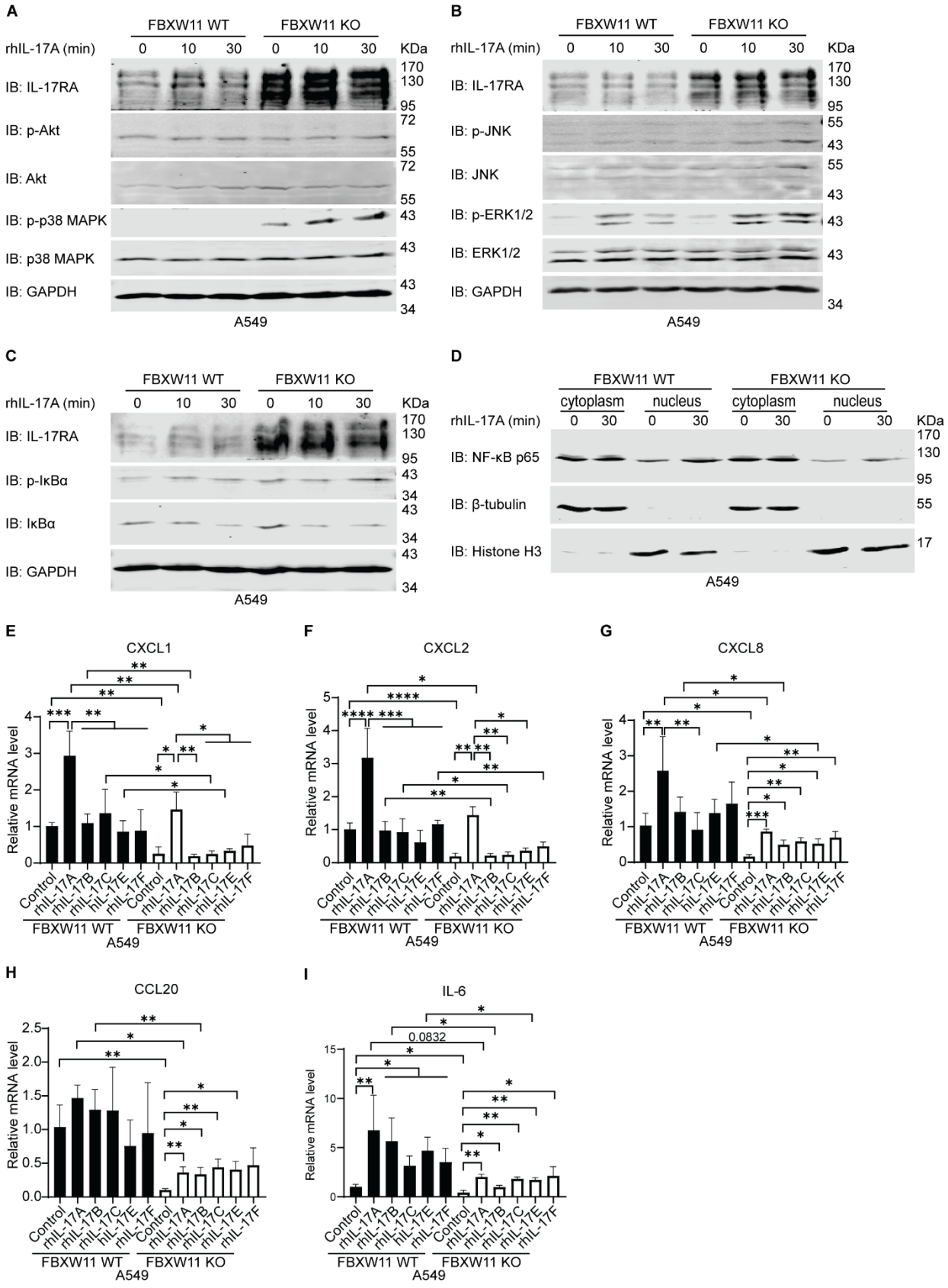

Figure 7. Knock-out of FBXW11 suppresses expression of IL-17-downstream genes through inhibiting nuclear entry of NF-κB p65.

(A-C) Western blot analysis of IL-17RA, phosphorylated AKT (p-AKT), AKT, phosphorylated p38 MAPK (p-p38 MAPK), p38 MAPK, phosphorylated JNK (p-JNK), JNK, phosphorylated ERK1/2 (p-ERK1/2), phosphorylated IκBα (p-IκBα) and IκBα. 2 x 10^6 A549 FBXW11 WT cells and 2.5 x 10^6 A549 FBXW11 KO cells were treated with 20 ng/ml rhIL-17A for 10 min and 30 min, while the control cells were treated with 0.1% BSA. **(D)** Western blot analysis of NF-κB p65 in cytoplasmic and nuclear extracts. 2 x 10^6 A549 FBXW11 WT cells and 2.5 x 10^6 A549 FBXW11 KO cells were treated with 20 ng/ml rhIL-17A for 30 min, while the control cells were treated with 0.1% BSA. Experiments were repeated 6 times independently. **(E-I)** Induction of IL-17-downstream gene expression. A549 FBXW11 WT and FBXW11 KO cells were treated with 20 ng/ml recombinant human IL-17 (rhIL-17) cytokines, including rhIL-17A, rhIL-17B, rhIL-17C, rhIL-17E, and rhIL-17F, for 2 h. Expression of CXCL1 **(E)**, CXCL2 **(F)**, CXCL8 **(G)**, CCL20 **(H)**, and IL-6 **(I)** was evaluated using real-time qPCR analysis, normalized to internal GAPDH control. The cells treated with 0.1% bovine serum albumin (BSA) were used as calibration control. Fold change of each target gene over control is shown. Error bar represents mean $\pm$ standard deviation (S.D.). The student's *t* test was used to calculate statistical significance of fold change. * $P < 0.05$, ** $P < 0.01$, *** $P < 0.001$, and **** $P < 0.0001$. Experiments were repeated 3 times independently.

Figure 7-figure supplement 1.

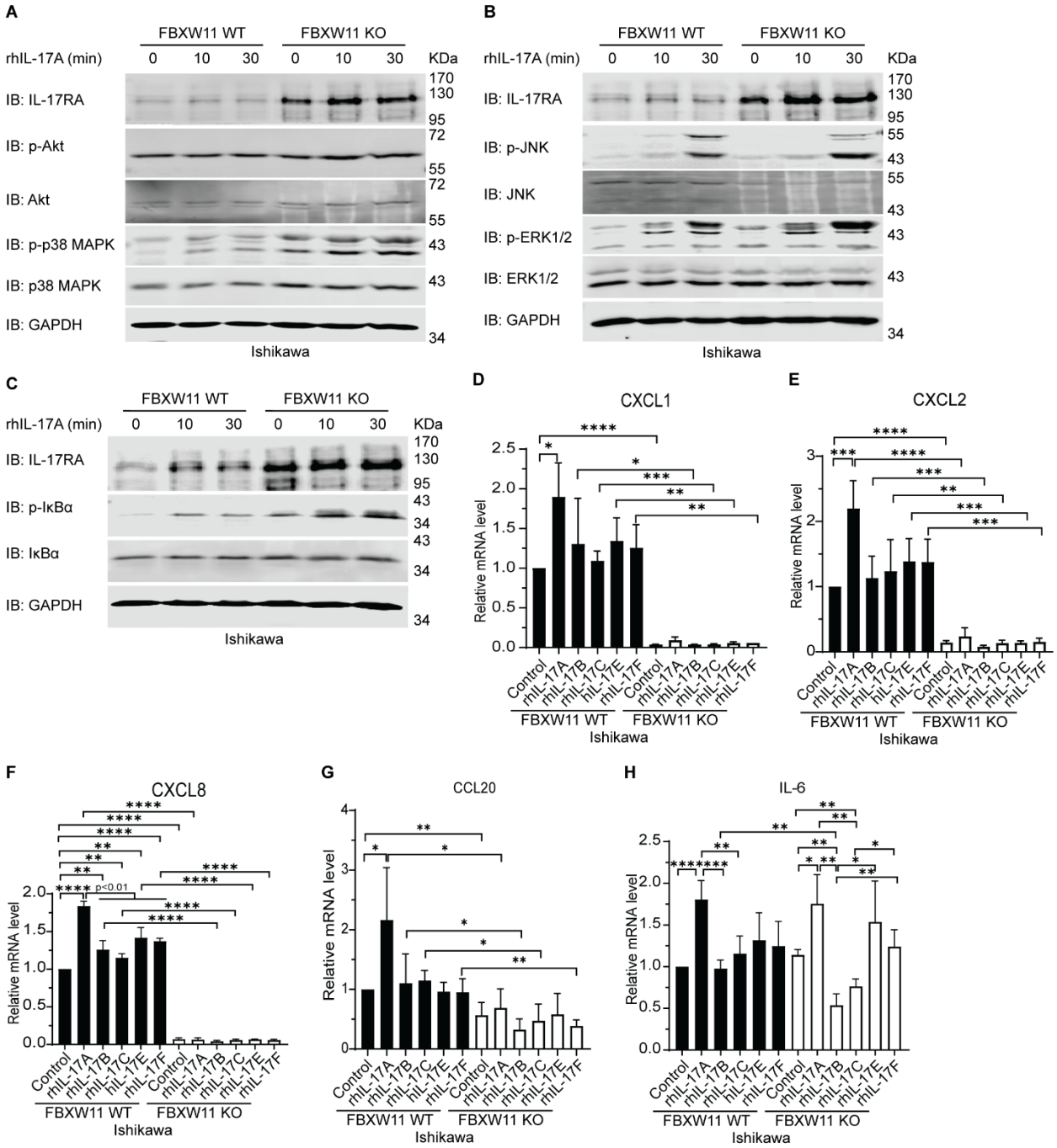

Figure 7-figure supplement 1. Knock-out of FBXW11 suppresses expression of IL-17-downstream genes.

(A-C) Western blot analysis of IL-17RA, phosphorylated AKT (p-AKT), AKT, phosphorylated p38 MAPK (p-p38 MAPK), p38 MAPK, phosphorylated JNK (p-JNK), JNK, phosphorylated ERK1/2 (p-ERK1/2), phosphorylated IκBα (p-IκBα) and IκBα. 2 x 10^6 Ishikawa FBXW11 WT cells and 2.5 x 10^6 Ishikawa FBXW11 KO cells were treated with 20 ng/ml rhIL-17A for 10 min and 30 min, while the control cells were treated with 0.1% BSA. Experiments were repeated at least 5 times independently. **(D-H)** Induction of IL-

17-downstream gene expression. Ishikawa FBXW11 WT and FBXW11 KO cells were treated with 20 ng/ml recombinant human IL-17 (rhIL-17) cytokines, including rhIL-17A, rhIL-17B, rhIL-17C, rhIL-17E, and rhIL-17F, for 2 h. Expression of CXCL1 **(D)**, CXCL2 **(E)**, CXCL8 **(F)**, CCL20 **(G)**, and IL-6 **(H)** was evaluated using real-time qPCR analysis, normalized to internal GAPDH control. The cells treated with 0.1% bovine serum albumin (BSA) were used as calibration control. Fold change of each target gene over control is shown. Error bar represents mean $\pm$ standard deviation (S.D.). The student's *t* test was used to calculate statistical significance of fold change. * $P < 0.05$, ** $P < 0.01$, *** $P < 0.001$, and **** $P < 0.0001$. Experiments were repeated 3 times independently.

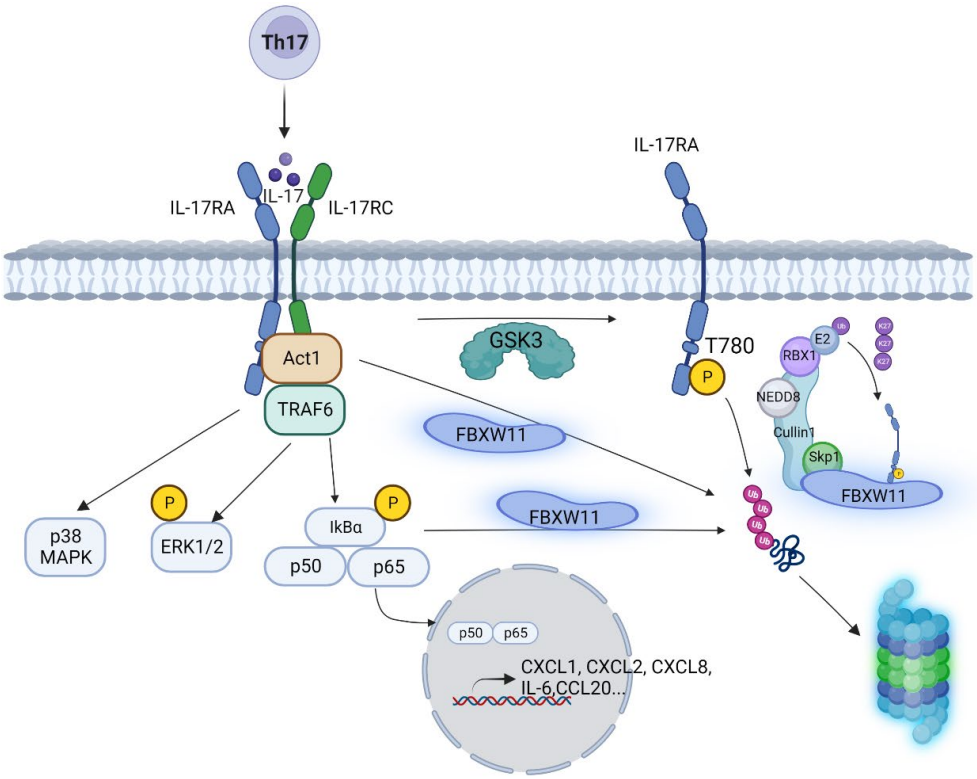

Figure 8. SCF^{FBXW11} complex regulates IL-17 signaling at multiple levels, including IL-17RA, Act1, and IκBα.

IL-17A, interleukin-17A; IL-17RA, interleukin-17 receptor A; IL-17RC, interleukin-17 receptor C; Act1, NF-κB-activated protein 1; TRAF6, tumor-necrosis factor receptor-associated factor 6; Ub, ubiquitin; IκBα, NF-κB inhibitor α; p50 and p65, NF-κB subunits; p38 MAPK,p38 mitogen-activated protein kinase; ERK1/2, extracellular signal-regulated kinase 1/2; IL-6, interleukin-6; CXCL1, C-X-C motif ligand 1; CXCL2, C-X-C motif ligand 2; CXCL8, C-X-C motif ligand 8; CCL20, C-C motif ligand 20; GSK3, Glycogen Synthase Kinase; E2, ubiquitin conjugation enzyme E2; RBX1, Ring-Box 1; NEDD8, Neural Precursor Cell Expressed, Developmentally Down-Regulated 8; Skp1, S-Phase Kinase Associated Protein 1; FBXW11, F-Box and WD Repeat Domain Containing 11. Illustration was made using BioRendor.

1256 **Table**

1257 **Table 1: Primers used in Real-time qPCR.**

Gene name	Primers (synthesized by Eurofins Genomics)
hCXCL1	Forward: 5′-AACCGAAGTCATAGCCACAC-3′
	Reverse: 5-GTTGGATTTGTCACTGTTCAGC-3′
hCXCL2	Forward: 5′-CTGCGCTGCCAGTGCTT-3′
	Reverse: 5′-CCTTCACACTTTGGATGTTCTTGA-3′
hCXCL8	Forward: 5′-GTGCAGTTTTGCCAAGGAGT-3′
	Reverse: 5′-CTCTGCACCCAGTTTTCCTT-3′
hCCL20	Forward: 5′-TGCTGTACCAAGAGTTTGCTC-3′
	Reverse: 5′-CGCACACAGACAACTTTTTCTTT-3′
hIL-6	Forward: 5′-GGTACATCCTCGACGGCATCT-3′
	Reverse: 5′-GTGCCTCTTTGCTGCTTTCAC-3′
hFBXW11	Forward: 5′-GTGGGATGTGAACACGGGTGA-3′
	Reverse: 5′-CGTAAAGTGATGTCGGTCGCAG-3′
hGAPDH	Forward: 5′-CCATGGGGAAGGTGAAGGTC-3′
	Reverse: 5′-AGTGATGGCATGGACTGTGG-3′

1258